J. Phys. G: Nucl. Part. Phys. **23** (1997) A1–A69. Printed in the UK PII: S0954-3899(97)82177-9

DATA REVIEW

A compilation of data on single and double prompt photon production in hadron–hadron interactions

W Vogelsang†§ and M R Whalley‡

† Rutherford Appleton Laboratory, Chilton, Didcot OX11 0QX, UK

‡ Department of Physics, Science Laboratories, University of Durham, Durham DH1 3LE, UK

Received 26 February 1997

Abstract. A compilation of all the available data on single prompt photon production in hadron–hadron interactions is presented, in both tabular and graphical form. An interpretation of these data in terms of the 'state-of-the-art' NLO theory is described with specific emphasis on the uncertainties involved. Comparisons of this theory with the individual data sets are made in order to indicate to the reader the scope and general status of the available data. For completeness, data on two-prompt-photon production are also included in a separate small section. All the data in this review can be found in and retrieved from the Durham–RAL HEP Databases together with data on a wide variety of other reactions.

Contents

§ Now at: Theory Division, CERN, CH-1211 Geneva 23, Switzerland

0954-3899/97/070001+69$19.50

1. Introduction

1.1. General remarks

The production of high-p_T prompt photons in hadronic collisions is an important testing ground for perturbative QCD. This is due primarily to the relatively clean signal provided by photons and their point-like electromagnetic coupling to quarks, enabling a probe of the dynamics of the underlying hard-scattering subprocesses that involve the strong interactions. The presence and dominance of the leading order (LO) $\mathcal{O}(\alpha\alpha_s)$ 'Compton-like' subprocess $qg \to \gamma q$ has made single prompt photon production $AB \to \gamma X$ an invaluable probe of the gluon distributions of the interacting hadrons A, B.

Experimentally, prompt photon production has been most widely studied in pp and $\bar{\text{p}}$p interactions. Here data have been taken in fixed target experiments [5, 7, 10, 12] as well as at the ISR [13–15, 17, 18] $S\text{p}\bar{\text{p}}S$ [20–22] and Tevatron [23, 25] colliders. As a result, the prompt photon data for proton-(anti)proton scattering cover the kinematical range $0.01 \lesssim x_T \equiv 2p_T/\sqrt{s} \lesssim 0.6$ quite well. Data with $0.2 \lesssim x_T \lesssim 0.6$ have also been published for fixed target experiments with pion beams [2, 3, 5, 8, 11] and/or nucleus (N = Be, C) [1–3, 11] targets. The simultaneous production of two-photons has also been measured for similar beam/target configurations [4, 6, 9, 16, 19–22, 24].

Since the advent of the first data on hadronic direct-γ production, considerable theoretical progress has been made in the sense that it has become possible to perform a complete and fully consistent next-to-leading order (NLO) QCD calculation of the prompt photon cross section. Calculations of the QCD corrections to the (dominant) so-called 'direct' subprocesses have been published in [26–29]. The (sub-dominant) fragmentation contribution can be calculated to NLO owing to [30] in which the corrections to all partonic $2 \to 2$ 'pure-QCD' subprocesses have been provided, and to the determination of NLO sets of parton-to-photon fragmentation functions in [31, 32]. In addition, the development of a proper NLO theoretical implementation of isolation cuts [33, 27], imposed on the cross section in the high-energy $S\text{p}\bar{\text{p}}S$ and Tevatron experiments, was completed fairly recently [34] and demonstrated to be phenomenologically important [35]. Subsequently, constraints on the proton's gluon distribution were derived from a combined analysis of the prompt photon and DIS data in [36], extending previous pioneering work of [37].

As was shown in [36], quite substantial uncertainties still remain in the theory calculation of the prompt photon cross section even to NLO. Among these are, most notably, the dependence of the theoretical cross section on unphysical scales, such as the renormalization scale μ_R and the factorization scale μ_F, and the ambiguities originating from the experimentally virtually unknown parton-to-photon fragmentation functions. When comparing experimental data with theory it is crucial to keep in mind such uncertainties inherent to the calculation along with the experimental errors.

It is the purpose of this review to provide a compilation of all available experimental data on hadronic prompt photon production. At the same time, a comparison with the 'state-of-the-art' NLO theory calculation will always be given to provide an assessment of the agreement between data and theory and to facilitate comparisons between different data sets. We organize the work as follows: the remainder of this introduction sets the general framework for all theory calculations. More specifically, in subsection 1.2 we will summarize the main ingredients needed to calculate the inclusive and isolated prompt photon cross sections in NLO. Subsection 1.3 is devoted to a detailed discussion of the main theoretical uncertainties mentioned above and their effects on the calculated cross sections. Much of the results presented in this subsection was taken from [36]. In section 1.4 we

briefly collect all input quantities used for the final theory calculations to be compared to the data. Following a brief description of the data tables in subsection 1.5, the actual data tables and plots for single prompt photon production are in section 2. For completeness, section 3 compiles all double photon data.

1.2. General framework

Two types of processes contribute to the prompt photon production cross section: the so-called 'direct' piece, where the photon is emitted via a pointlike (direct) coupling to a quark, and the fragmentation piece, in which the photon originates from the fragmentation of a final state parton (see figure 1).

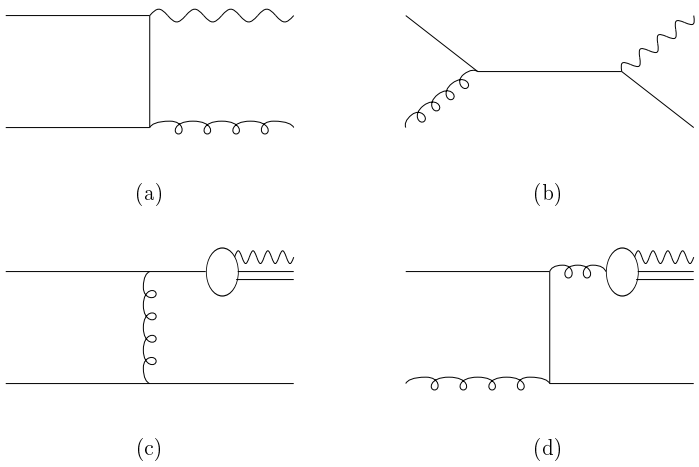

Figure 1. LO examples of direct ((a), (b)) and fragmentation ((c), (d)) contributions to the prompt photon cross section.

Despite the fact that its corresponding partonic subprocesses are of order α_s^2, the fragmentation contribution is present already in LO since the parton-to-photon fragmentation functions are effectively of order α/α_s in perturbative QCD, where α denotes the fine structure constant. Next order corrections in the strong coupling constant α_s have been calculated in the $\overline{\text{MS}}$ renormalization and factorization schemes for both the direct [26–29] and the fragmentation [30] subprocesses, hence the cross sections can be consistently calculated to order $\alpha\alpha_s^2$. The cross section for the fully inclusive production of a single prompt photon with momentum p_γ schematically reads

$$d\sigma_{AB} \equiv d\sigma_{\text{dir}} + d\sigma_{\text{frag}} = \sum_{a,b=q,\bar{q},g} \int \mathrm{d}x_a \mathrm{d}x_b f_a^A(x_a,\mu_F^2) f_b^B(x_b,\mu_F^2) \times \Bigg[d\hat{\sigma}_{ab}^{\gamma}(p_\gamma, x_a, x_b, \mu_R, \mu_F, M_F) + \sum_{c=q,\bar{q},g} \int_{z_{\min}}^1 \frac{\mathrm{d}z}{z^2} d\hat{\sigma}_{ab}^{c}(p_\gamma, x_a, x_b, z, \mu_R, \mu_F, M_F) D_c^{\gamma}(z, M_F^2) \Bigg] \tag{1}$$

where $z_{\min} = x_T \cosh\eta$ with the prompt photon's rapidity η, and $x_T = 2p_T/\sqrt{s}$. In equation (1), $d\hat{\sigma}_{ab}^{i}$ represent the subprocess cross sections for partons a, b producing a

particle i ($i = \gamma, q, g$), integrated over the full phase space of all other final state particles. $f_i^A(x, \mu_F^2)$ denotes the number density of the parton type i in hadron A at momentum fraction x and scale μ_F, and $D_c^\gamma(z, M_F^2)$ is the photon fragmentation function at scale M_F, z being the fraction of energy of the fragmenting parton c transferred to the photon.

As already mentioned in the introduction and made explicit in equation (1), the cross section in any fixed order of perturbation theory depends on unphysical scales which have to be introduced in the procedure of renormalization (μ_R) and of factorization of initial (μ_F) and final (M_F) state mass singularities. The latter type of singularities appears, for example, in the calculation of the $\mathcal{O}(\alpha_s^3)$ $ab \to cde$ NLO fragmentation subprocess cross sections when the parton c (which then fragments into the photon) becomes collinear with particle d or e, but also in the calculation of the $\mathcal{O}(\alpha\alpha_s^2)$ $ab \to \gamma de$ NLO 'direct' subprocess cross sections when the photon and a final state quark are collinear. These singularities need to be factorized at a scale M_F into the 'bare' fragmentation functions in order to render the cross section finite. The fragmentation functions then obey corresponding NLO evolution equations. Since factorizing singularities is not a unique procedure but depends on the factorization prescription adopted, it becomes obvious that only the sum of the direct and the fragmentation pieces is a physical (scheme independent) quantity beyond the LO, but not these parts individually. Needless to say that a consistent NLO calculation also affords hadronic parton distributions evolved to NLO.

At the very high-energy $\bar{\mathrm{p}}\mathrm{p}$ colliders the photon is experimentally required to be 'isolated' in order to suppress the huge background due to copious production of π^0, whose decay can fake a prompt photon event. This is usually achieved by demanding that the amount of hadronic energy E_{had} allowed in a cone $\sqrt{(\Delta\phi)^2 + (\Delta\eta)^2} \leqslant R$ around the photon direction is limited to a small fraction of the photon energy, $E_{\mathrm{had}} \leqslant \epsilon E_\gamma$ with $\epsilon \lesssim 0.1$. In order to compare QCD predictions with isolated collider data, the theoretical calculation has to include this isolation criterion which leads to a significant decrease from the fully inclusive cross section [34, 38]. In [34] a simple, yet accurate way of incorporating the isolation cut into the NLO calculation has been developed. Starting from the fully inclusive cross section, the isolated one is obtained by writing [33, 34],

$$d\sigma^{\mathrm{isol}}(R, \epsilon) = d\sigma^{\mathrm{incl}} - d\sigma^{\mathrm{sub}}(R, \epsilon) \tag{2}$$

where $d\sigma^{\mathrm{sub}}(R, \epsilon)$ is a subtraction cross section. In case of the NLO direct contributions, $d\sigma^{\mathrm{sub}}(R, \epsilon)$ represents the cross section for having *more* hadronic energy than ϵE_γ in the cone around the photon. It turns out that $d\sigma^{\mathrm{sub}}(R, \epsilon)$ can be easily and reliably calculated under the assumption of a rather narrow cone. The very good accuracy of this approximation for cone sizes of up to $R = 1$ and prompt photon rapidities of $|\eta| < 1$ was recently demonstrated within a new Monte Carlo calculation [29] of the NLO direct piece†. An equation similar to equation (2) can also be written down for the NLO fragmentation piece [34], in which case the main effect of imposing the isolation cut is to raise the lower integration limit in equation (1) to $z_{\mathrm{min}} = 1/(1 + \epsilon)$. In this way, it is possible to calculate also the *isolated* prompt photon production cross section measured at high-energy colliders in a consistent way beyond the leading order. We note at this point that it was recently claimed [39] that factorization breaks down for the isolated prompt photon cross section due to uncancelled infrared singularities appearing in the calculation. This claim has, however, been contested in [40, 29].

† We note that in [29] also a long-standing $\mathcal{O}(10\%)$ discrepancy between the NLO programs of [26, 28] and [27] for the direct part was resolved. All NLO calculations of this part of the prompt photon cross section are in agreement now.

For all calculations to follow we use the program of [28] for the direct part of the NLO prompt photon cross section, along with the expressions of [30] for the fragmentation contribution. When calculating the isolated cross section we complement these programs according to the prescription of [34].

1.3. Theoretical uncertainties

In this subsection we address the main uncertainties entering the NLO calculation of the prompt photon cross section, namely the dependence on the photon fragmentation functions and on the renormalization and mass factorization scales. As a point of reference, we first calculate the cross section for a fixed 'standard' set of input distributions and parameters and, for more illustrative purposes, confront it with a few data sets which are representative of the various kinematical regions explored by the hitherto performed pp and $\bar{\mathrm{p}}$p prompt photon experiments. For this purpose, the parton distributions and photon fragmentation functions are taken from GRV [41, 32], along with the accompanying values for the QCD scale parameter $\Lambda^{(f)}_{\overline{\mathrm{MS}}}$ for a given number f of active flavours. We choose $\mu_R = \mu_F = M_F = p_T/2$ for the renormalization and factorization scales except for the isolated prompt photon data, where $M_F = Rp_T$ seems more appropriate [33].

The very small charm effects in the cross section at fixed-target and ISR energies are neglected. For the $S\mathrm{p}\bar{\mathrm{p}}S$ and the Tevatron experiments, however, charm-induced contributions coming, for example, from $cg \to \gamma c$ are not negligible. We employ the effective (massless) charm quark distribution of [42] in calculating these contributions. It turns out [36] that reasonable variations of this charm density do not significantly alter the results. An alternative approach to the heavy quark (charm) contribution is to perform mass factorization only for the light u, d, and s quarks. In this scheme, also used in [41], the heavy flavours c, $b, \ldots$ do not act as partons in the proton, and in LO charmed prompt photon events are only introduced via the processes $gg \to \gamma c\bar{c}$ and $q\bar{q} \to \gamma c\bar{c}$ with *massive* charm quarks. The results of [43] show, however, that these two approaches yield very similar results at least in LO (for a NLO study of the prompt photon plus charm cross sections within the 'massless' approach see [44]). Thus the theoretical uncertainty originating from the charm treatment seems to be rather small. For the rest of this section and in all later calculations based on GRV parton distributions, we therefore use the fixed intrinsic charm quark distribution of [42] which facilitates the calculations.

The sets of experimental data we take into account for the moment are from pp and $\bar{\mathrm{p}}$p scattering only. Here we pick the combined fixed-target data of WA70 [7] ($\sqrt{s} = 24$ GeV, pp inclusive), the ISR results from R807 [18] ($\sqrt{s} = 63$ GeV, pp inclusive), the $S\mathrm{p}\bar{\mathrm{p}}S$ results from UA2 [20] ($\sqrt{s} = 630$ GeV, $\bar{\mathrm{p}}$p isolated) and the Tevatron data of CDF [23] ($\sqrt{s} = 1.8$ TeV, $\bar{\mathrm{p}}$p isolated). We follow precisely the experimental procedures of averaging the cross section over the prompt photon's transverse momentum p_T and its rapidity η; details will be given in the next subsection. We add the statistical and systematic errors in quadrature, using point-to-point errors where these are separately available. Figure 2 displays the results for our 'standard' choice of input distributions and parameters. We show the 'default quantity' $(D - T)/T$, i.e., (data $-$ theory)/theory versus x_T. This provides a particularly easy visualization of the (dis)agreement between data and theoretical calculation in view of the strong p_T fall-off of the cross section. x_T is a good representative of the Bjørken-x values predominantly probed in the parton distributions at given p_T and $\sqrt{s}$.

As can be seen from figure 2, the overall agreement between data and the NLO theoretical prediction is good though not complete, at least not within our 'standard' calculation. The agreement between theory and the fixed-target and ISR measurements

is very good, whereas the comparison with the high-energy collider results seems to be slightly less successful, since both the CDF and the UA2 data show a somewhat stronger rise for small x_T than the theoretical cross section. This effect is more pronounced and statistically more meaningful for the CDF results, which possess the smallest point-to-point errors of all data sets and therefore provide a very precise measurement of the *slope* of the cross section. It has to be emphasized that a *much* stronger discrepancy between high-energy collider data and NLO calculations was reported previously [23]. As was shown in [35], a strong improvement is obtained by using 'modern' sets of (steep) parton distribution functions like, for example, those of GRV [41, 42] or the recent MRS(A′,G) sets [45] as well as, equally important, by including a properly isolated NLO fragmentation contribution in the calculation. According to figure 2, the latter amounts to a 20% slope effect for CDF conditions, thus its inclusion is clearly crucial for a quantitative comparison between the experimental and theoretical cross sections. The fragmentation piece is non-negligible *despite* the presence of the isolation cut without which it would easily contribute about 50% to the total cross section [31, 35, 38]. Figure 2 also demonstrates that fragmentation also plays an important role in the calculations in the ISR and fixed-target regions, where no isolation cut has been applied. Here it leads to an effect of about 20% at some values of p_T, but influences the slope to a lesser extent.

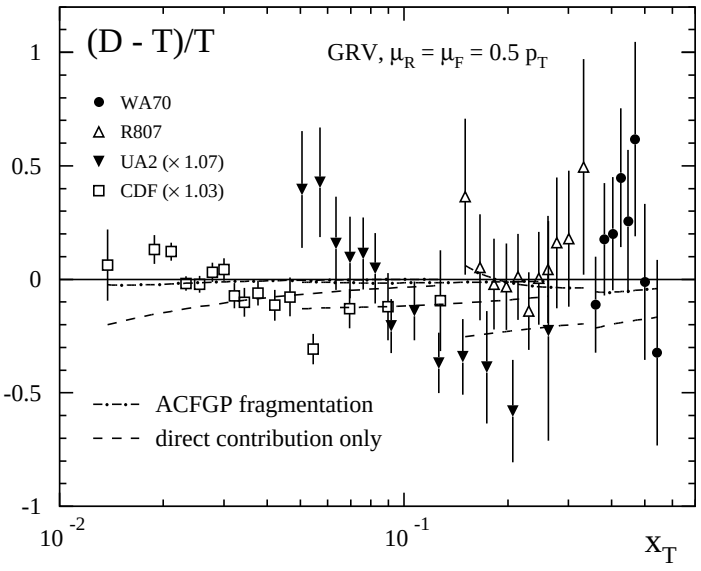

Figure 2. The 'default quantity' $(D-T)/T$ against $x_T = 2p_T/\sqrt{s}$ for the data of [7, 18, 20, 23] as compared to the NLO theoretical cross section T, using the GRV parton distributions and photon fragmentation functions [41, 32]. The curves present the shifts $(T' - T)/T$, where T' denotes the theoretical cross section if the fragmentation contribution is neglected or if the fragmentation functions of [31] are used. Note that the CDF [23] as well as the UA2 [20] data are subject to a normalization uncertainty of about 10% which we have used in the figure to center the results on the zero line.

The results in figure 2 indicate a remaining discrepancy between the p_T-slopes of the experimental and theoretical cross sections even after the improvements of [35] have been applied. An explanation for this discrepancy have been brought forward [46, 47] in terms of possibly relevant effects from additional partonic k_T-smearing. In [46] a reasonable

description of the data was achieved by assuming a Gaussian k_T-smearing for the partons; however, a very large average intrinsic k_T of $\sim$ 3–4 GeV for the $S\mathrm{p\bar{p}}S$ and Tevatron data was needed. In [47] the k_T-smearing arising from hard multiparton emissions (corresponding to even higher-order contributions) was estimated by merging the NLO QCD calculation with a parton shower algorithm. Again, an improved agreement between the $S\mathrm{p\bar{p}}S$ and Tevatron data and theory resulted. On the other hand, as was shown in [36], it is possible to obtain a good description of the prompt photon data within a global NLO analysis of DIS and direct-γ data by essentially fine-tuning the proton's gluon distribution. Hence in the present situation and in view of the quite sizeable theoretical uncertainties to be discussed below, it seems reasonable to stick to the 'pure' NLO perturbative QCD framework for carrying out the comparisons with data to be presented below.

An important uncertainty in the calculation is the dependence of the cross section on the parton-to-photon fragmentation functions which are experimentally unknown so far. Two partly very different NLO sets of such distributions have been suggested in the literature, namely in [31] (ACFGP) and in [32] (GRV). In both [31] and [32], the fragmentation functions are assumed to evolve from a pure vector meson dominance (VMD) input at some very low scale. However, this boundary condition for $D_i^\gamma(z, Q^2)$ has been implemented in rather different factorization schemes. ACFGP use the $\overline{\mathrm{MS}}$ scheme, whereas GRV impose the VMD input in the timelike version of the so-called DIS_γ scheme, originally introduced for the (spacelike) parton structure of the photon [48]. In the $\overline{\mathrm{MS}}$ scheme employed here the latter ansatz corresponds to an additional, rather large input for D_q^γ, which guarantees the positivity of the timelike structure function $f_1^{(T)}$ for single photon inclusive $\mathrm{e^+e^-}$ annihilation, $\mathrm{e^+e^-} \to \gamma X$. Thus the quark-to-photon fragmentation functions of GRV [32] are larger than the ones of ACFGP [31], especially at low scales, despite the fact that in [31] a sizeably larger VMD input is employed. On the other hand, D_g^γ of ACFGP is much larger than its GRV counterpart which is due to a huge VMD gluonic input in [31].

As is obvious from figure 2, the ACFGP [31] and GRV [32] fragmentation functions nevertheless yield very similar results for the total fragmentation contribution. For the isolated Tevatron case, $g \to \gamma$ fragmentation plays an almost negligible role due to the high $z_{\min}$ cut implied by the isolation criterion, for example, $z_{\min} = (1 + 2\ \mathrm{GeV}/p_T)^{-1}$ for CDF conditions. The $q \to \gamma$ pieces are rather similar, since $D_q^\gamma(z, Q^2)$ is probed at large z and Q^2 here. In the fully inclusive ISR case, on the other hand, $z_{\min} = x_T = 2p_T/\sqrt{s} \gtrsim 0.15$ for $\eta = 0$, and the huge difference in D_g^γ between [31] and [32] enters the fragmentation cross section. However, since the scales $Q^2 \approx p_T^2/4$ are rather low here, this effect is strongly compensated by the difference in the quark contributions. Of course, the difference in the total results is not necessarily fully representative of the uncertainty originating in the fragmentation part of the cross section. It was checked in [36] that in the theoretically more realistic GRV [32] case, a 50% change in the VMD input distributions for D_i^γ has no sizeable effect on the results due to the dominance of D_q^γ. Hence we will keep the fragmentation functions of [32] for the rest of this paper. Clearly, experimental information on the fragmentation functions, for example from $\mathrm{e^+e^-} \to \gamma X$ [49], is needed.

Let us now discuss the scale dependence of the results, i.e. the changes in the theoretical predictions for varying μ_R and μ_F. It turns out that the NLO cross section depends only *very* weakly on M_F both for the isolated [34] and the fully inclusive cases. For the latter, for example, the difference of the results for $M_F = p_T/2$ and $M_F = p_T$ at fixed μ_R, μ_F does not exceed 1%. We therefore keep the fragmentation scale M_F fixed at $M_F = p_T/2$ for the fixed-target and ISR experiments and $M_F = Rp_T$ for the isolated cross sections in the following. The dashed and the dash–dotted lines in figure 3 display

the shifts in the theoretical results if we choose $\mu_R = \mu_F = 0.3\,p_T$ or $\mu_R = \mu_F = 1.0\,p_T$, respectively, instead of $\mu_R = \mu_F = p_T/2$. More precisely, the curves show $(T' - T)/T$, where T' is the theoretical cross section as calculated with the new values for the scales, whereas T corresponds to the 'standard' calculation. It becomes obvious that the results for $\mu_R = \mu_F = 0.3\,p_T$ or $1.0\,p_T$ amount to almost a constant shift in the normalization of the theoretical cross section as far as the CDF and UA2 data are concerned, and do not provide a change in the slope of the cross section. It can also be seen that the theoretical cross section at lower energies shows a rather strong scale dependence.

As was discussed in [36], the situation changes somewhat if one allows μ_R and μ_F to be different. A smaller renormalization scale μ_R along with a larger factorization scale μ_F can be expected to create a steeper slope of the theoretical result, since lowering μ_R mainly increases the strong coupling constant α_s, whereas the main effect of a larger μ_F is to deplete the gluon distribution at larger x and to increase it at smaller x. In fact, the curves in figure 3 show that these effects are quite significant. The choices of, for example, $\mu_R = 0.3\,p_T$, $\mu_F = p_T$ or $\mu_R = p_T$, $\mu_F = 0.3\,p_T$ do lead to about $\pm 20\%$ shape changes in the CDF region, respectively. Thus, obviously, scale dependences are in general also able to affect the p_T-*slope* of the NLO cross section.

All in all, scale changes seem to have a rather strong influence on the theoretical cross section even beyond the LO and appear to be the dominant source of uncertainty. This finding is in line with the early observations in [33], where it was shown that at small x_T the scale dependence is only slightly reduced when going from LO to NLO, which renders it difficult to estimate the most appropriate scales. The scale dependence of the NLO cross section for prompt photon production indicates the importance of corrections of even higher order and also sets severe limits on the possibility to derive conclusions, concerning, for example, the proton's gluon distribution, from these data [36].

1.4. Introductory remarks about the comparison with the data

After the discussion of the main theoretical uncertainties inherent to the NLO calculation of the direct-γ cross section, we can now proceed to choose all input parameters and densities for the global comparison of data and theory that will accompany the actual compilation of all data.

Our calculations will rather closely follow the standard one in the last subsection. For instance, we will now fix the renormalization and factorization scales at $\mu_R = \mu_F = M_F = p_T/2$, except for $M_F = Rp_T$ for the isolated data. Also, we will again use the GRV NLO photon fragmentation functions [32] throughout. For the proton structure functions we will use a set of each of the major 'collaborations' that have provided NLO distributions. These will be set A′ of MRS [45], the 1994 GRV set [41], and the CTEQ-2M distributions [50]. In this way we can at the same time assess the (rather small) additional theoretical uncertainty coming from this source. When calculating the cross sections (per nucleon) for interactions with the isoscalar targets N = Be, C we simply average over the proton and neutron cross sections, N (per nucleon) $= (p + n)/2$. We do not attempt to take into account any possible nuclear effects. For the case of experiments employing pion beams we use the pionic parton distributions of GRV [51] and MRSS [52]. We do not calculate a CTEQ prediction in this case as no suitable parton distribution is available. We always choose the values for the QCD scale parameter $\Lambda^{(f)}_{\overline{\rm MS}}$ according to the proton parton densities employed in the calculation, with f increasing by one unit at each heavy flavour threshold. For instance, for $f = 4$ flavours this means $\Lambda^{(4)}_{\overline{\rm MS}} = 231,\ 200,\ 213$ MeV for the MRS-A′, GRV and CTEQ-2M parton sets, respectively. Charm contributions to the cross section are

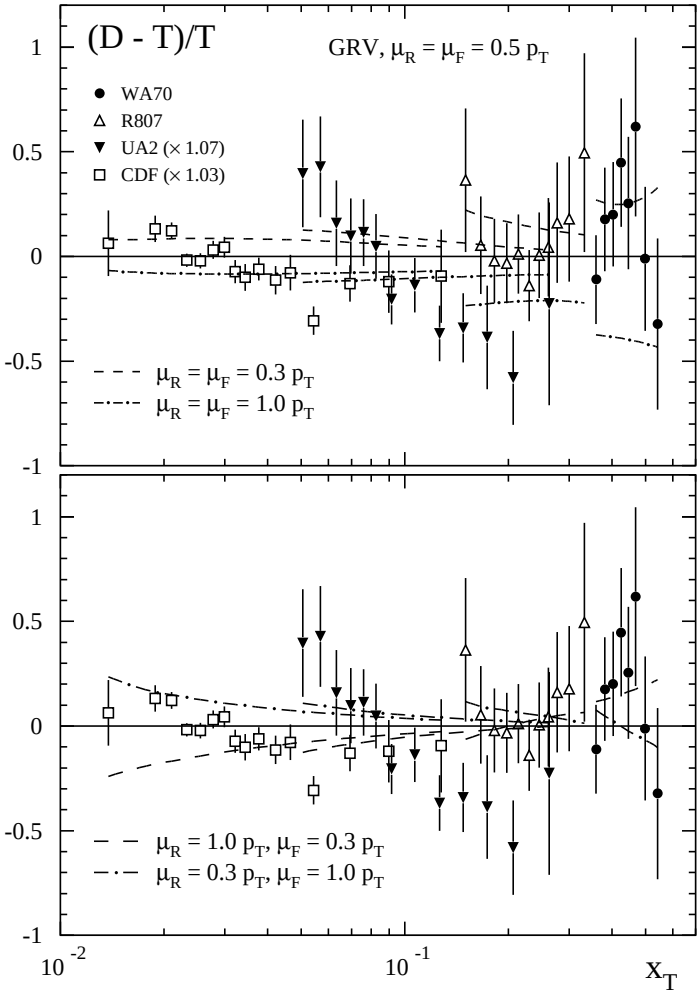

Figure 3. Same as for figure 2, but the lines displaying the shifts in the theoretical results if the renormalization and factorization scales are varied as indicated in the figure.

neglected for fixed target energies, but included in the collider regime by employing the 'massless' charm quark distributions provided in the various sets (see also the discussion in subsection 1.3 for the GRV set). Even heavier flavours are neglected throughout. We note that for some fixed target experiments our above choice for μ_R, μ_F, M_F leads to scales slightly below the minimally allowed values for the MRS and CTEQ parton sets. We ignore this small inconsistency arising here and just use the distributions as returned by the respective parametrisations, which implies a freezing of the parton densities for $Q^2 < 4$ GeV^2 in case of the MRS set and an extrapolation to $Q^2 < 2.56$ GeV^2 in the case of the CTEQ distributions. Our results for such corresponding p_T should be considered with some

care here. In case of the GRV distributions the input scale is so low that no problem of this kind occurs.

When dealing with the isolated prompt photon cross section as measured at the $S\bar{p}pS$ and Tevatron colliders we again try to match the experimental isolation criteria as closely as possible. For this purpose we use the following parameters:

- $R = 0.7$, $\epsilon = \min(2\ \mathrm{GeV}/p_T, 0.1)$ for UA1 [22],
- $R = 0.53$, $\epsilon = 2\ \mathrm{GeV}/p_T$ and $R = 0.265$, $\epsilon \approx 0.25$ for the UA2 data in [21] and [20], respectively,
- $R = 0.7$, $\epsilon = 2\ \mathrm{GeV}/p_T$ for CDF [23],
- $R_1 = 0.2$, $\epsilon_1 = 1/24$ and $R_2 = 0.4$, $\epsilon_2 = 2\ \mathrm{GeV}/p_T$ for D0 [25]. In this experiment the isolation is achieved by defining two cones characterized by R_1, ϵ_1 and R_2, ϵ_2 with restrictions on the allowed hadronic energy in the cone annulus as well as in the inner cone.

In order to fully consistently account for the experimental definition of the differential cross sections we average the the theoretical ones over the respective p_T and η bins accessed in the experiment, i.e.,

$$\langle \mathcal{D}\sigma \rangle \equiv \frac{1}{p_T^+ - p_T^-} \int_{p_T^-}^{p_T^+} \mathrm{d}p_T \ \frac{1}{y_+ - y_-} \int_{y_-}^{y_+} \mathrm{d}y \ \mathcal{D}\sigma \tag{3}$$

where $\mathcal{D}\sigma$ stands for any differential cross section, for instance, $\mathcal{D} = E\mathrm{d}^3/\mathrm{d}p^3$ for most fixed target experiments or $\mathcal{D} = \mathrm{d}^2/\mathrm{d}p_T/\mathrm{d}\eta$ for the Tevatron experiments, and where in most cases $y = \eta$ except for the WA70 and E704 experiments where $y = x_F = x_T \cosh\eta$. When comparing theory with data it then appears the best choice [53] to put the data point at the position p_T^0 (or η^0, x_F^0) where the averaged and the local theory value coincide, i.e., where

$$\langle \mathcal{D}\sigma \rangle \equiv \mathcal{D}\sigma(p_T^0, y^0) \ . \tag{4}$$

This will be done for all plots in the graphs to follow in section 2. The smooth theory curves shown in section 2 are obtained calculating the cross section locally at the respective p_T values, but averaging over rapidity as done in the experiment (and vice versa for cross sections shown versus η or x_F).

1.5. The data

In the next section the measurements of all prompt photon production differential cross sections are tabulated as well as being displayed graphically. The data are ordered primarily by initial state as follows,

- p p $\to \gamma$ X
- $\bar{\mathrm{p}}$ p $\to \gamma$ X
- p nucleus $\to \gamma$ X
- π^+ p $\to \gamma$ X
- π^- p $\to \gamma$ X
- π^+ nucleus $\to \gamma$ X
- π^- nucleus $\to \gamma$ X

and then in increasing values of centre-of-mass energy. It is assumed that the results from later publications supersede those of earlier ones by the same experiment and therefore only the latest results have been included here. However earlier papers are generally listed

in the bibliographic references at the end. Any additional p_T independent systematic or normalization uncertainties are mentioned in the captions in the individual tables. The reader is referred to the original publications for details of experimental conditions, cuts, resolutions and discussion of systematic errors which may affect data comparison.

As outlined earlier in this section, we have included in each individual plot the predictions of the latest theory using the three common structure function parametrisations (CTEQ-2M, GRV-94 and MRS-A′). The purpose of this is not specifically to test the validity of, and difference between, the predictions. It is, rather, to be able to compare the different data sets each of which is measured not only at different beam momenta, but also with different ranges in p_T and $\eta(x_F,y)$. Direct comparison is difficult and the theory curves serve to provide a common 'base-line'. As well as the p_T scale on the bottom axis of each plot the corresponding x_T scale is also given along the top axis. The small insets in each plot show the 'default' quantity $(D-T)/T$ for each data set. In these insets, for clarity, only the MRS-A′ comparison is shown. The only exception to this is for the Fermilab E629 data where GRV is shown as the p_T region is too low for MRS-A′ to be applicable.

We begin section 2 with an index of the single prompt photon data which gives the beam, target and kinematical ranges covered. At the end of section 2 we show, for each initial state, a combined $(D-T)/T$ plot to show how the different data sets compare with one another. These are similar to the two plots earlier in this section the difference being that they contain *all* the data and not a selected few. Section 3 covers two-photon data and again begins with a data index. The section is included for completeness and no attempt to provide any theoretical interpretation is made here.

This compilation is intended to be comprehensive, and we apologise for the omission of any data sets which may have been overlooked.

2. The single photon data

Table 1. Data on single prompt photon production.

Collaboration	$\sqrt{s}$ GeV	Beam	Target	x_T range ($= 2p_T/\sqrt{s}$)	y, η, x_F range
†E95 [1]	19.40, 23.75	p	Be	$0.15 < x_T < 0.45$	$-0.7 < y < 0.7$
E629 [2]	19.40	p, π^+	C	$0.22 < x_T < 0.52$	$-0.75 < y < 0.2$
NA3 [3]	19.40	p, $\pi^\pm$	C	$0.26 < x_T < 0.62$	$-0.4 < y < 1.2$
E704 [10]	19.40	p	p	$0.26 < x_T < 0.39$	$-0.15 < x_F < 0.15$
NA24 [5]	23.75	p, $\pi^\pm$	p	$0.23 < x_T < 0.59$	$-0.65 < y < 0.52$
WA70 [7, 8]	22.96	p, $\pi^\pm$	p	$0.35 < x_T < 0.61$	$-0.35 < x_F < 0.55$
UA6 [12]	24.3	p, $\bar{\text{p}}$	p	$0.34 < x_T < 0.50$	$-0.2 < y < 1.0$
E706 [11]	30.63	p, π^-	Be	$0.20 < x_T < 0.65$	$-0.7 < y < 0.7$
R108 [13]	62.4	p	p	$0.17 < x_T < 0.42$	$-0.45 < y < 0.45$
R110 [14]	63.0	p	p	$0.14 < x_T < 0.29$	$-0.8 < y < 0.8$
R806 [15]	63.0	p	p	$0.12 < x_T < 0.38$	$-0.2 < y < 0.2$
†R807 [17]	53.0	p, $\bar{\text{p}}$	p	$0.11 < x_T < 0.23$	$-0.4 < y < 0.4$
R807 [18]	63.0	p	p	$0.15 < x_T < 0.33$	$-0.7 < y < 0.7$
UA2 [20, 21]	630	$\bar{\text{p}}$	p	$0.04 < x_T < 0.32$	$-0.76 < \eta < 0.76$ $1.0 < \lvert\eta\rvert < 1.8$
UA1 [22]	546, 630	$\bar{\text{p}}$	p	$0.05 < x_T < 0.29$	$-0.8 < \eta < 0.8$ $0.8 < \lvert\eta\rvert < 1.4$ $1.6 < \lvert\eta\rvert < 3.0$
E741(CDF) [23]	1800	$\bar{\text{p}}$	p	$0.010 < x_T < 0.13$	$-0.9 < \eta < 0.9$
E740(D0) [25]	1800	$\bar{\text{p}}$	p	$0.01 < x_T < 0.12$	$-0.9 < \eta < 0.9$ $1.6 < \lvert\eta\rvert < 2.5$

† γ/π^0 ratio only.

Table 2. The invariant cross section for single prompt photon production in proton–proton collisions at incident beam momentum 200 GeV/c, as a function of the photon's transverse momentum, in the region $|x_F| < 0.15$, as measured by the Fermilab E704 experiment. There is an additional 12% normalization uncertainty.

FNAL E704	p p $\to \gamma$ X	$\sqrt{s} = 19.4$ GeV
Adams *et al* 1995		*Phys. Lett.* **345B** 569

$\lvert x_F \rvert$	p_T (GeV/c)	$\langle p_T \rangle$ (GeV/c)	$\langle x_T \rangle$	$E\mathrm{d}^3\sigma/\mathrm{d}p^3$ (pb/GeV^2)
<0.15	2.5–2.7	2.59	0.267	4900 ± 610 ± 490
	2.7–2.9	2.79	0.288	1580 ± 380 ± 250
	2.9–3.1	2.99	0.308	1150 ± 270 ± 130
	3.1–3.4	3.24	0.334	539 ± 160 ± 59
	3.4–3.8	3.59	0.370	312 ± 91 ± 27

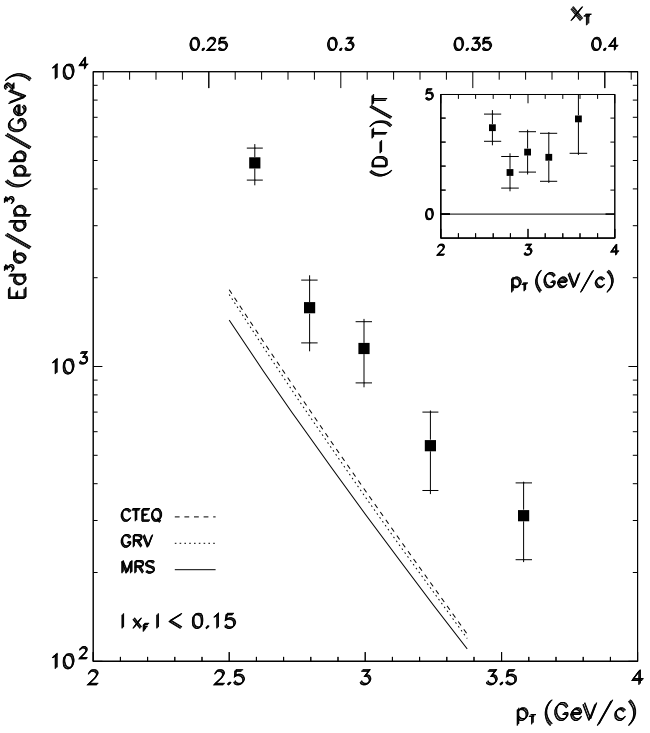

Figure 4. The E704 proton–proton prompt photon p_T distribution. The theoretical predictions are displayed together with the $(D - T)/T$ comparison in the inset.

Table 3. The invariant cross section for single prompt photon production in proton–proton collisions at incident beam momentum 280 GeV/c, as a function of the photon's transverse momentum,in eight x_F regions from −0.35 to 0.45, as measured by the CERN WA70 experiment.

CERN WA70 Bonesini *et al* 1988	p p → γ X			$\sqrt{s} = 22.96$ GeV *Z. Phys.* C **38** 371
x_F	p_T (GeV/c)	$\langle p_T \rangle$ (GeV/c)	$\langle x_T \rangle$	$E\mathrm{d}^3\sigma/\mathrm{d}p^3$ (pb/GeV^2)
−0.35 – −0.25	4.00–4.25	4.11	0.358	22.605 ± 3.991 ± 6.825
	4.25–4.50	4.36	0.380	9.453 ± 3.198 ± 4.452
	4.50–5.00	4.70	0.409	5.902 ± 1.227 ± 1.575
	5.00–5.50	5.20	0.453	2.822 ± 0.784 ± 0.773
−0.25 – −0.15	4.00–4.25	4.11	0.358	31.353 ± 4.406 ± 8.607
	4.25–4.50	4.36	0.380	22.878 ± 2.863 ± 5.030
	4.50–5.00	4.70	0.409	8.381 ± 1.473 ± 2.006
	5.00–5.50	5.20	0.453	1.972 ± 0.649 ± 0.570
	5.50–6.00	5.70	0.497	0.663 ± 0.372 ± 0.249
−0.15 – −0.05	4.00–4.25	4.11	0.358	29.649 ± 4.000 ± 8.197
	4.25–4.50	4.36	0.380	24.883 ± 3.324 ± 5.672
	4.50–5.00	4.70	0.409	10.215 ± 1.425 ± 2.128
	5.00–5.50	5.20	0.453	2.869 ± 0.705 ± 0.682
	5.50–6.00	5.70	0.497	0.720 ± 0.344 ± 0.243
−0.05 – 0.05	4.00–4.25	4.11	0.358	32.612 ± 3.930 ± 8.481
	4.25–4.50	4.36	0.380	23.988 ± 3.254 ± 5.712
	4.50–5.00	4.70	0.409	10.540 ± 1.375 ± 2.139
	5.00–5.50	5.20	0.453	3.920 ± 0.867 ± 0.944
	5.50–6.00	5.70	0.497	0.683 ± 0.320 ± 0.218
0.05 – 0.15	4.00–4.25	4.11	0.358	19.926 ± 3.661 ± 7.173
	4.25–4.50	4.36	0.380	19.358 ± 4.285 ± 6.839
	4.50–5.00	4.70	0.409	9.383 ± 1.636 ± 2.233
	5.00–5.50	5.20	0.453	2.346 ± 0.622 ± 0.606
	5.50–6.00	5.70	0.497	0.662 ± 0.331 ± 0.228
0.15 – 0.25	4.00–4.25	4.11	0.358	19.945 ± 3.995 ± 7.152
	4.25–4.50	4.36	0.380	17.509 ± 2.836 ± 4.328
	4.50–5.00	4.70	0.409	8.773 ± 1.412 ± 1.916
	5.00–5.50	5.20	0.453	2.115 ± 0.579 ± 0.530
	5.50–6.00	5.70	0.497	0.588 ± 0.335 ± 0.240
0.25 – 0.35	4.00–4.25	4.11	0.358	11.954 ± 2.685 ± 3.635
	4.25–4.50	4.36	0.380	6.539 ± 2.057 ± 2.707
	4.50–5.00	4.70	0.409	5.734 ± 1.182 ± 1.363
	5.00–5.50	5.20	0.453	1.692 ± 0.572 ± 0.466
	5.50–6.00	5.70	0.497	0.258 ± 0.218 ± 0.109
0.35 – 0.45	4.00–4.25	4.11	0.358	11.550 ± 3.526 ± 4.686
	4.25–4.50	4.36	0.380	4.465 ± 2.000 ± 2.113
	4.50–5.00	4.70	0.409	0.852 ± 0.685 ± 0.578
	5.00–5.50	5.20	0.453	0.946 ± 0.701 ± 0.504

Table 4. The invariant cross section for single prompt photon production in proton–proton collisions at incident beam momentum 280 GeV/c, as a function of the photon's transverse momentum, in four x_F regions from -0.35 to 0.45, as measured by the CERN WA70 experiment.

CERN WA70 Bonesini *et al* 1988	p p $\rightarrow \gamma$ X			$\sqrt{s} = 22.96$ GeV *Z. Phys.* C **38** 371
x_F	p_T (GeV/c)	$\langle p_T \rangle$ (GeV/c)	$\langle x_T \rangle$	$E\mathrm{d}^3\sigma/\mathrm{d}p^3$ (pb/GeV^2)
-0.35 – 0.45	4.00–4.25	4.11	0.358	22.039 ± 1.278 ± 5.096
	4.25–4.50	4.36	0.380	15.781 ± 0.993 ± 3.164
	4.50–4.75	4.61	0.402	8.744 ± 0.710 ± 1.669
	4.75–5.00	4.86	0.423	5.720 ± 0.539 ± 1.083
	5.00–5.25	5.11	0.445	2.683 ± 0.362 ± 0.568
	5.25–5.50	5.36	0.467	1.861 ± 0.288 ± 0.399
	5.50–6.00	5.70	0.497	0.463 ± 0.104 ± 0.123
	6.00–6.50	6.20	0.540	0.086 ± 0.042 ± 0.030
-0.35 – -0.15	4.00–4.25	4.11	0.358	26.994 ± 2.939 ± 6.703
	4.25–4.50	4.36	0.380	17.187 ± 2.045 ± 3.829
	4.50–4.75	4.61	0.402	8.893 ± 1.594 ± 2.234
	4.75–5.00	4.86	0.423	5.460 ± 1.078 ± 1.330
	5.00–5.50	5.20	0.453	2.314 ± 0.486 ± 0.626
	5.50–6.00	5.70	0.497	0.435 ± 0.214 ± 0.192
	6.00–6.50	6.20	0.540	0.266 ± 0.154 ± 0.197
-0.15 – 0.15	4.00–4.25	4.11	0.358	27.341 ± 2.226 ± 6.821
	4.25–4.50	4.36	0.380	21.207 ± 1.873 ± 4.590
	4.50–4.75	4.61	0.402	11.481 ± 1.252 ± 2.304
	4.75–5.00	4.86	0.423	7.434 ± 0.972 ± 1.517
	5.00–5.25	5.11	0.445	3.472 ± 0.658 ± 0.793
	5.25–5.50	5.36	0.467	2.629 ± 0.559 ± 0.604
	5.50–6.00	5.70	0.497	0.669 ± 0.191 ± 0.207
	6.00–6.50	6.20	0.540	0.215 ± 0.097 ± 0.108
0.15 – 0.45	4.00–4.25	4.11	0.358	13.969 ± 1.863 ± 3.821
	4.25–4.50	4.36	0.380	9.511 ± 1.323 ± 2.230
	4.50–4.75	4.61	0.402	5.949 ± 1.030 ± 1.356
	4.75–5.00	4.86	0.423	4.195 ± 0.799 ± 0.945
	5.00–5.50	5.20	0.453	1.494 ± 0.306 ± 0.386
	5.50–6.00	5.70	0.497	0.317 ± 0.144 ± 0.113
	6.00–6.50	6.20	0.540	0.028 ± 0.035 ± 0.016

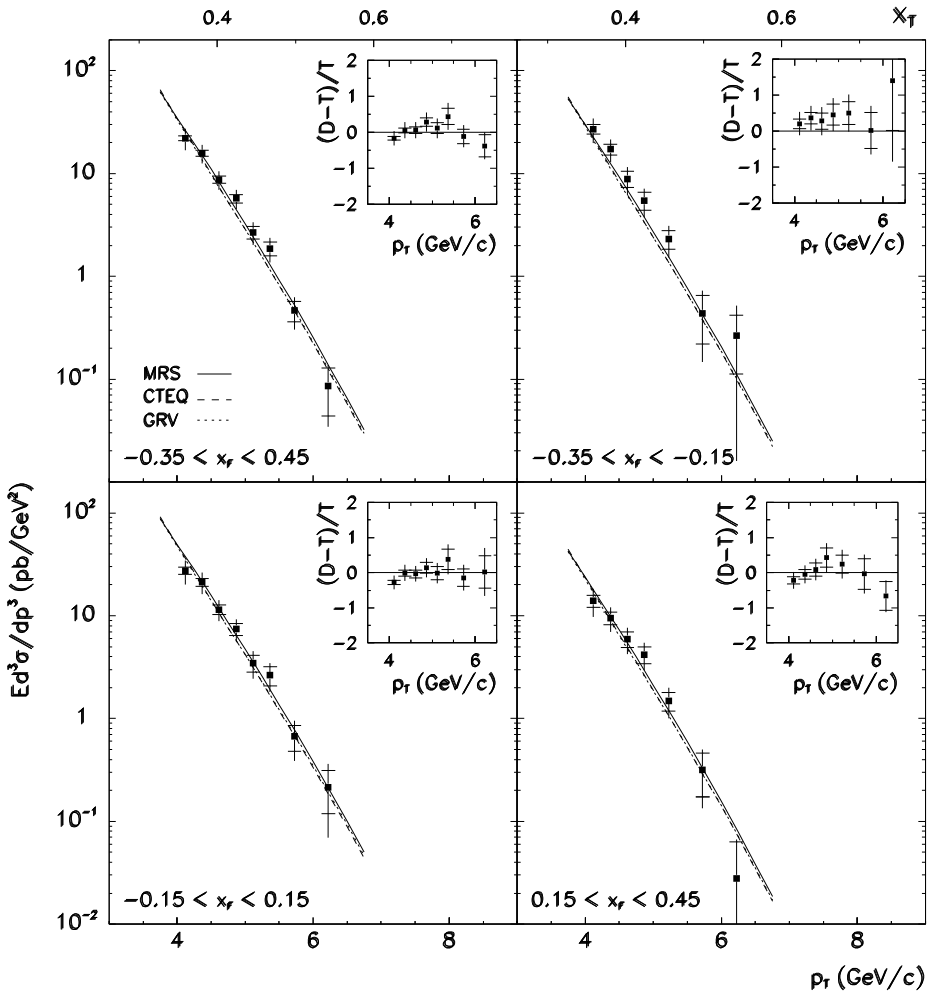

Figure 5. The WA70 proton–proton prompt photon p_T distributions for the wider x_F bin data. The theoretical predictions are displayed together with the $(D-T)/T$ comparisons in the insets.

Table 5. The invariant cross section for single prompt photon production in proton–proton collisions at incident beam momentum 280 GeV/c, as a function of x_F in three p_T ranges, as measured by the CERN WA70 experiment.

CERN WA70 Bonesini *et al* 1988		p p $\rightarrow \gamma$ X	$\sqrt{s} = 22.96$ GeV *Z. Phys.* C **38** 371
p_T (GeV/c)	$\langle x_F \rangle$	x_F	$E\mathrm{d}^3\sigma/\mathrm{d}p^3$ (pb/GeV^2)
4.0–4.5	−0.30	−0.35 – −0.25	16.356 ± 2.576 ± 4.673
	−0.20	−0.25 – −0.15	27.643 ± 2.614 ± 6.337
	−0.10	−0.15 – −0.05	27.183 ± 2.598 ± 6.442
	0.00	−0.05 – 0.05	28.156 ± 2.544 ± 6.621
	0.10	0.05 – 0.15	17.034 ± 2.411 ± 5.361
	0.20	0.15 – 0.25	19.028 ± 2.445 ± 5.061
	0.30	0.25 – 0.35	9.272 ± 1.689 ± 2.612
	0.40	0.35 – 0.45	7.580 ± 1.965 ± 2.634
4.5–5.0	−0.30	−0.35 – −0.25	5.902 ± 1.227 ± 1.575
	−0.20	−0.25 – −0.15	8.381 ± 1.473 ± 2.006
	−0.10	−0.15 – −0.05	10.215 ± 1.425 ± 2.128
	0.00	−0.05 – 0.05	10.540 ± 1.375 ± 2.139
	0.10	0.05 – 0.15	9.383 ± 1.636 ± 2.233
	0.20	0.15 – 0.25	8.773 ± 1.412 ± 1.916
	0.30	0.25 – 0.35	5.734 ± 1.182 ± 1.363
	0.40	0.35 – 0.45	0.852 ± 0.685 ± 0.578
5.0–6.0	−0.30	−0.35 – −0.25	1.485 ± 0.395 ± 0.383
	−0.20	−0.25 – −0.15	1.299 ± 0.369 ± 0.339
	−0.10	−0.15 – −0.05	1.790 ± 0.392 ± 0.411
	0.00	−0.05 – 0.05	2.304 ± 0.459 ± 0.529
	0.10	0.05 – 0.15	1.484 ± 0.370 ± 0.365
	0.20	0.15 – 0.25	1.353 ± 0.333 ± 0.320
	0.30	0.25 – 0.35	0.968 ± 0.304 ± 0.248
	0.40	0.35 – 0.45	0.397 ± 0.324 ± 0.237

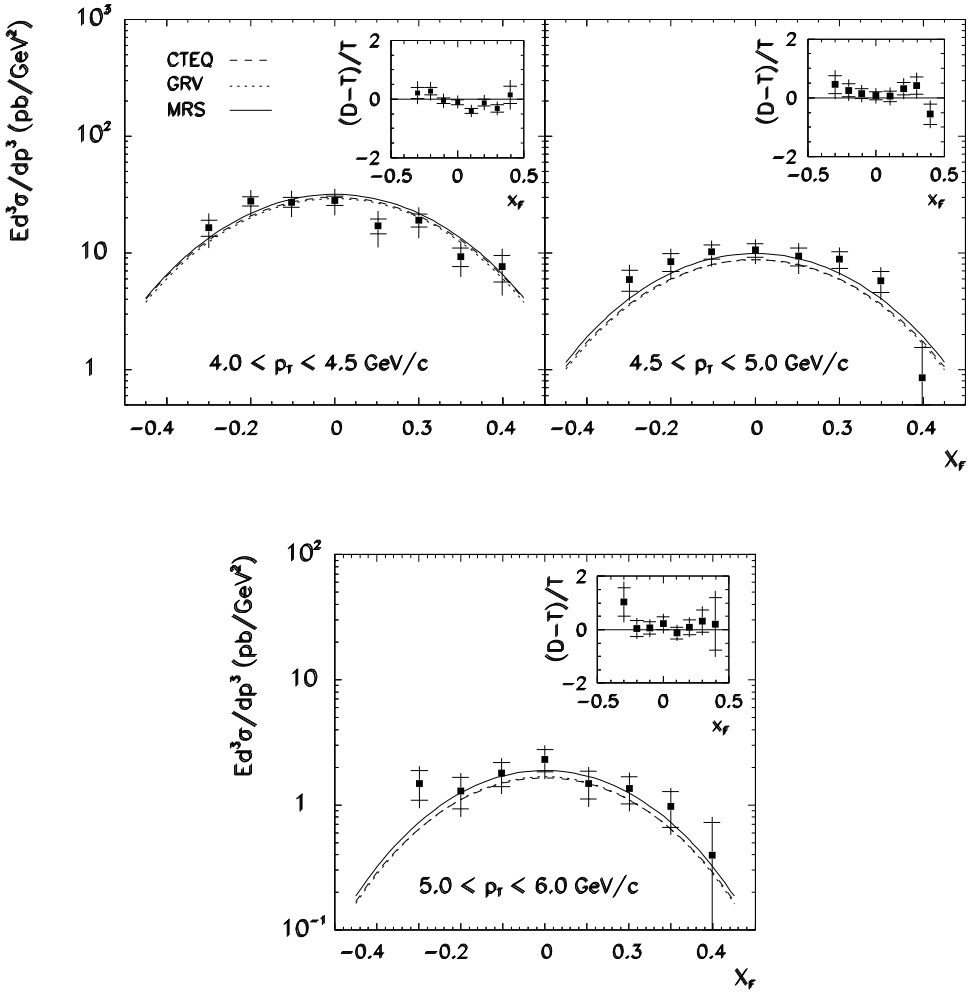

Figure 6. The WA70 proton–proton prompt photon x_F distributions for the three p_T ranges. The theoretical predictions are displayed together with the $(D-T)/T$ comparisons in the insets.

Table 6. The invariant cross section for single prompt photon production in proton–proton collisions at incident beam momentum 300 GeV/c, as a function of the photon's transverse momentum, in the region $-0.65 < y < 0.52$, as measured by the CERN NA24 experiment. The data have an additional 7% uncertainty in normalization and a 1% uncertainty in the momentum scale.

CERN NA24	p p $\rightarrow \gamma$ X	$\sqrt{s} = 23.75$ GeV
De Marzo *et al* 1987		*Phys. Rev.* D **36** 8

y	p_T (GeV/c)	$p_T^{\rm mid}$ (GeV/c)	$x_T^{\rm mid}$	$E{\rm d}^3\sigma/{\rm d}p^3$ (pb/GeV^2)
−0.65–0.52	3.0–3.5	3.25	0.274	375.0 ± 93.0 ± 170.0
	3.5–4.0	3.75	0.316	121.0 ± 39.0 ± 29.0
	4.0–4.5	4.25	0.358	25.0 ± 4.0 ± 7.5
	4.5–5.5	5.00	0.421	5.48 ± 1.20 ± 1.10
	5.5–6.5	6.00	0.505	0.950 ± 0.390 ± 0.060

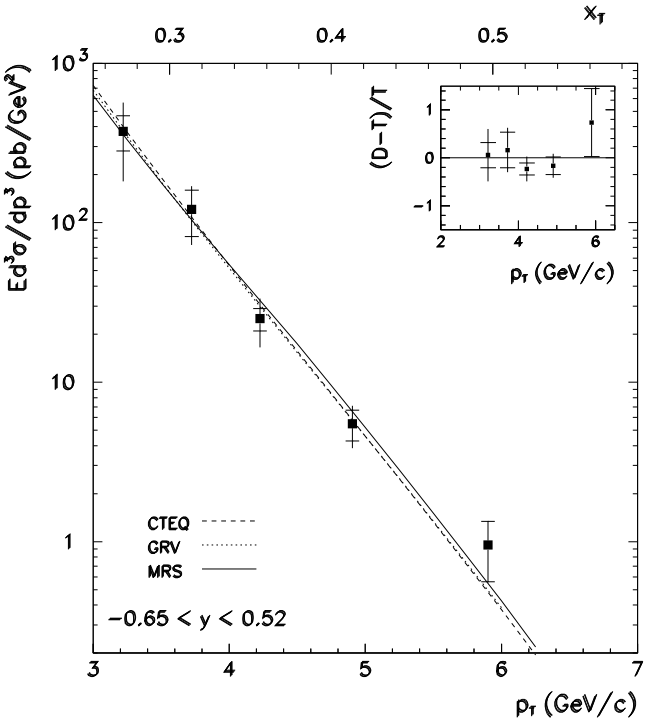

Figure 7. The NA24 proton–proton prompt photon p_T distribution. The theoretical predictions are displayed together with the $(D - T)/T$ comparison in the inset.

Table 7. The invariant cross section for single prompt photon production in proton–proton collisions at incident beam momentum 315 GeV/c, as a function of the photon's transverse momentum, in the region $-0.2 < y < 1.0$, as measured by the CERN UA6 experiment.

CERN UA6	p p → γ X	$\sqrt{s} = 24.30$ GeV
Ballocchi *et al* 1993		*Phys. Lett.* **317B** 250

y	p_T (GeV/c)	$p_T^{\rm mid}$ (GeV/c)	$x_T^{\rm mid}$	$E{\rm d}^3\sigma/{\rm d}p^3$ (pb/GeV^2)
−0.2–1.0	4.1–4.3	4.2	0.346	55.5 ± 13.7 ± 11.1
	4.3–4.5	4.4	0.362	28.9 ± 8.8 ± 5.8
	4.5–4.7	4.6	0.379	16.3 ± 6.6 ± 3.3
	4.7–4.9	4.8	0.395	9.6 ± 4.8 ± 1.9
	4.9–5.3	5.1	0.420	6.0 ± 2.0 ± 1.2
	5.3–6.1	5.7	0.469	1.2 ± 0.5 ± 0.2

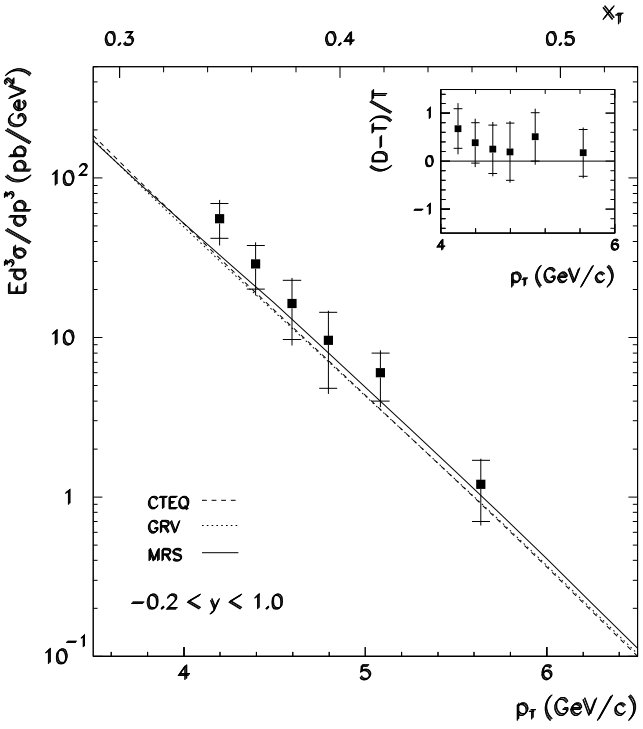

Figure 8. The UA6 proton–proton prompt photon p_T distribution. The theoretical predictions are displayed together with the $(D - T)/T$ comparison in the inset.

Table 8. The invariant cross section for single prompt photon production in proton–proton collisions at a centre-of-mass energy of 63 GeV, as a function of the photon's transverse momentum, in the region $|y| < 0.8$, as measured by the CERN ISR R110 experiment. The systematic errors range from 15% at the lowest p_T to 19% at the highest, with an additional overall scale uncertainty of 5%.

CERN R110	p p $\rightarrow \gamma$ X	$\sqrt{s} = 63.00$ GeV
Angelis *et al* 1989		*Nucl. Phys.* B **327** 541

y	p_T (GeV/c)	$\langle p_T \rangle$ (GeV/c)	$\langle x_T \rangle$	$E\mathrm{d}^3\sigma/\mathrm{d}p^3$ (pb/GeV^2)
−0.8–0.8	4.5– 5.0	4.72	0.150	225 ± 33
	5.0– 5.5	5.22	0.166	141 ± 42
	5.5– 6.0	5.72	0.182	65.6 ± 24.2
	6.0– 6.5	6.23	0.198	39.4 ± 6.3
	6.5– 7.0	6.73	0.214	19.6 ± 6.1
	7.0– 8.0	7.42	0.236	7.21 ± 2.72
	8.0–10.0	8.72	0.277	1.37 ± 0.86

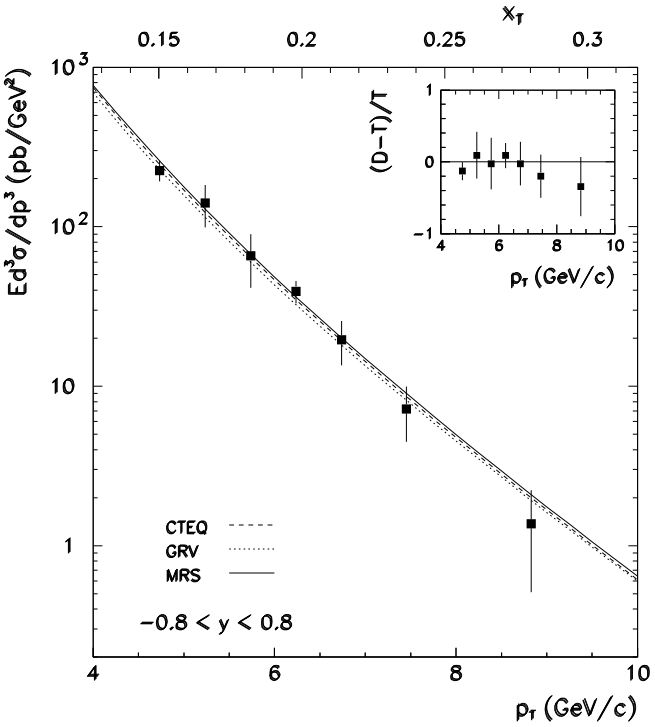

Figure 9. The R110 proton–proton prompt photon p_T distribution. The theoretical predictions are displayed together with the $(D - T)/T$ comparison in the inset.

Table 9. The invariant cross section for single prompt photon production in proton–proton collisions at a centre-of-mass energy of 63 GeV, as a function of the photon transverse momentum, in the region $|y| < 0.2$, as measured by the CERN ISR R806 experiment.

CERN R806 Anassontzis *et al* 1982	pp → γ X			$\sqrt{s} = 63.00$ GeV *Z. Phys.* C **13** 277	
y	p_T (GeV/c)	$p_T^{\rm mid}$ (GeV/c)	$x_T^{\rm mid}$	$E{\rm d}^3\sigma/{\rm d}p^3$ (pb/GeV^2)	
−0.2–0.2	3.5– 4.0	3.75	0.119	3070.0 ±	± 1690.0
	4.0– 4.5	4.25	0.138	977.0 ±	± 410.0
	4.5– 5.0	4.75	0.151	454.0 ± 5.0	± 145.0
	5.0– 5.5	5.25	0.167	200.0 ± 3.0	± 54.0
	5.5– 6.0	5.75	0.183	87.8 ± 2.2	± 21.9
	6.0– 6.5	6.25	0.198	40.8 ± 1.5	± 9.7
	6.5– 7.0	6.75	0.214	22.6 ± 1.1	± 5.1
	7.0– 7.5	7.25	0.230	10.8 ± 0.7	± 2.4
	7.5– 8.0	7.75	0.246	6.41 ± 0.60	± 1.42
	8.0– 8.5	8.25	0.262	3.84 ± 0.46	± 0.84
	8.5– 9.0	8.75	0.278	2.09 ± 0.32	± 0.46
	9.0–10.0	9.50	0.302	0.858 ± 0.153	± 0.196
	10.0–11.0	10.50	0.333	0.168 ± 0.052	± 0.048
	11.0–12.0	11.50	0.365	0.148 ± 0.058	± 0.035

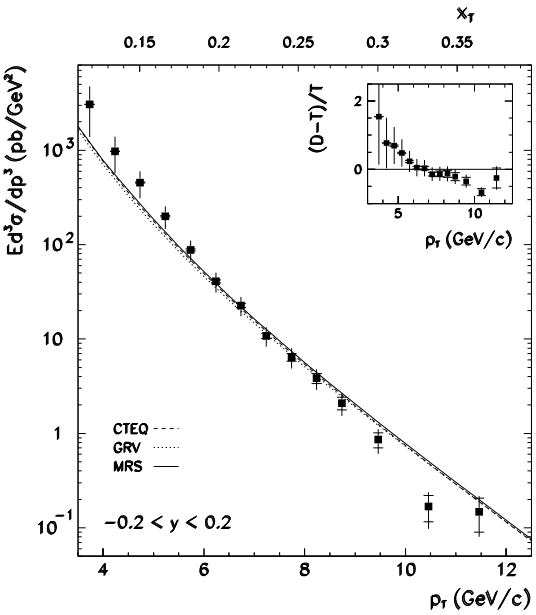

Figure 10. The R806 proton–proton prompt photon p_T distribution. The theoretical predictions are displayed together with the $(D - T)/T$ comparison in the inset.

Table 10. The invariant cross section for single prompt photon production in proton–proton collisions at a centre-of-mass energy of 63 GeV, as a function of the photon transverse momentum, at $\eta = 0.0$, as measured by the CERN ISR R807 experiment. Errors contain the systematic uncertainties.

CERN R807	p p $\rightarrow \gamma$ X			$\sqrt{s} = 63.00$ GeV
Åkesson *et al* 1990				*Sov. J. Nucl. Phys.* **51** 836
η	p_T (GeV/c)	$\langle p_T \rangle$ (GeV/c)	$\langle x_T \rangle$	$E\mathrm{d}^3\sigma/\mathrm{d}p^3$ (pb/GeV^2)
0.0	4.5– 5.0	4.75	0.151	314.0 ± 79.0
(−0.7–0.7)	5.0– 5.5	5.25	0.167	122.0 ± 27.0
	5.5– 6.0	5.73	0.182	59.6 ± 12.2
	6.0– 6.5	6.23	0.198	32.0 ± 6.3
	6.5– 7.0	6.74	0.214	18.7 ± 3.5
	7.0– 7.5	7.23	0.230	9.1 ± 1.8
	7.5– 8.0	7.72	0.245	6.20 ± 1.26
	8.0– 8.5	8.22	0.261	3.81 ± 0.86
	8.5– 9.0	8.74	0.277	2.54 ± 0.63
	9.0–10.0	9.44	0.300	1.260 ± 0.320
	10.0–11.0	10.36	0.329	0.605 ± 0.192

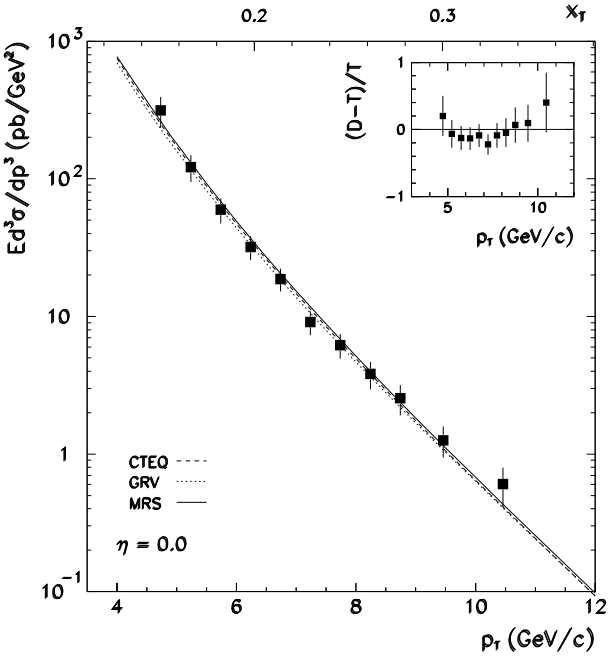

Figure 11. The R807 proton–proton prompt photon p_T distribution. The theoretical predictions are displayed together with the $(D - T)/T$ comparison in the inset.

Table 11. The invariant cross section for single prompt photon production in proton–antiproton collisions at incident beam momentum 315 GeV/c, as a function of the photon's transverse momentum, in the region $-0.2 < y < 1.0$, as measured by the CERN UA6 experiment.

CERN UA6	$\bar{\mathrm{p}}\ \mathrm{p} \to \gamma\ \mathrm{X}$	$\sqrt{s} = 24.30$ GeV
Ballocchi *et al* 1993		*Phys. Lett.* **317B** 250

y	p_T (GeV/c)	p_T^{mid} (GeV/c)	x_T^{mid}	$E\mathrm{d}^3\sigma/\mathrm{d}p^3$ (pb/GeV^2)
−0.2–1.0	4.1–4.3	4.2	0.346	119.1 ± 21.8 ± 17.9
	4.3–4.5	4.4	0.362	66.6 ± 15.1 ± 10.0
	4.5–4.7	4.6	0.379	44.6 ± 10.8 ± 6.7
	4.7–4.9	4.8	0.395	26.8 ± 8.1 ± 4.0
	4.9–5.3	5.1	0.420	7.7 ± 3.5 ± 1.2
	5.3–6.1	5.7	0.469	5.4 ± 1.4 ± 0.8

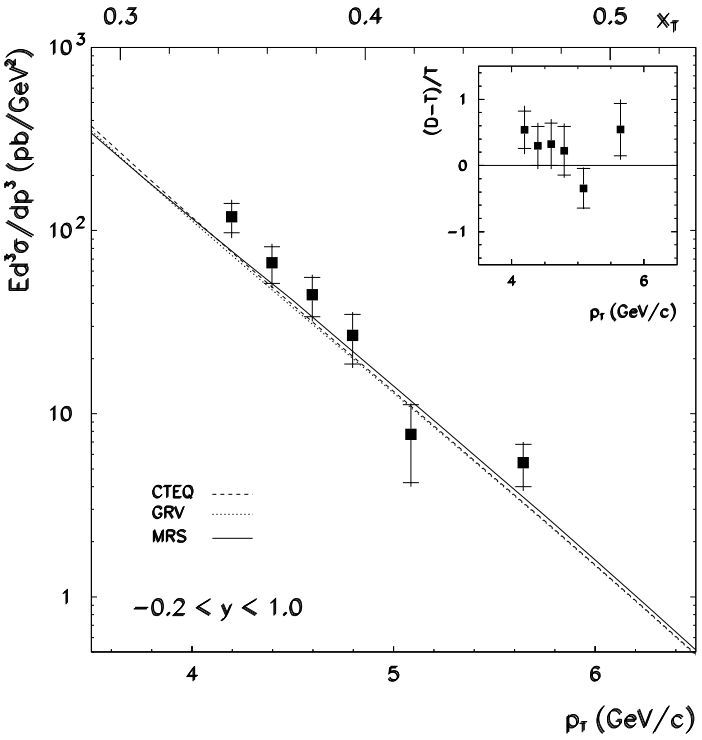

Figure 12. The UA6 proton–antiproton prompt photon p_T distribution. The theoretical predictions are displayed together with the $(D - T)/T$ comparison in the inset.

Table 12. The invariant cross section for single prompt photon production in proton–antiproton collisions at a centre-of-mass energy of 546 GeV, as a function of the photon's transverse momentum, in three pseudorapidity regions, $\eta = 0.0$, 1.1, and 2.3, as measured by the CERN UA1 experiment. These data are produced using a photon isolation cut as described in the introduction. There is also an additional 23% overall systematic uncertainty.

CERN UA1	$\bar{\mathrm{p}}\,\mathrm{p} \to \gamma\ \mathrm{X}$		$\sqrt{s} = 546$ GeV
Albajar *et al* 1988			*Phys. Lett.* **209B** 385
$\lvert\eta\rvert$	p_T^{mid} (GeV/c)	x_T^{mid}	$E\mathrm{d}^3\sigma/\mathrm{d}p^3$ (pb/GeV^2)
0.0	17.00	0.062	3.91 ± 0.37 ± 0.44
(−0.8–0.8)	19.00	0.070	1.74 ± 0.24 ± 0.17
	21.00	0.077	1.12 ± 0.19 ± 0.10
	25.00	0.092	0.38 ± 0.06 ± 0.03
	34.50	0.126	0.049 ± 0.013 ± 0.002
	46.00	0.168	0.0084 ± 0.0060 ± 0.0002
1.1	17.00	0.062	2.42 ± 0.32 ± 0.35
(0.8–1.4)	19.00	0.070	1.47 ± 0.24 ± 0.20
	21.00	0.077	0.82 ± 0.17 ± 0.11
	25.00	0.092	0.231 ± 0.048 ± 0.029
	37.00	0.136	0.0113 ± 0.0046 ± 0.0015
2.3	16.50	0.060	0.75 ± 0.13 ± 0.23
(1.6–3.0)	18.50	0.068	0.36 ± 0.05 ± 0.10
	21.50	0.079	0.125 ± 0.026 ± 0.035
	24.50	0.090	0.038 ± 0.013 ± 0.010
	32.00	0.117	0.0017 ± 0.0006 ± 0.0005

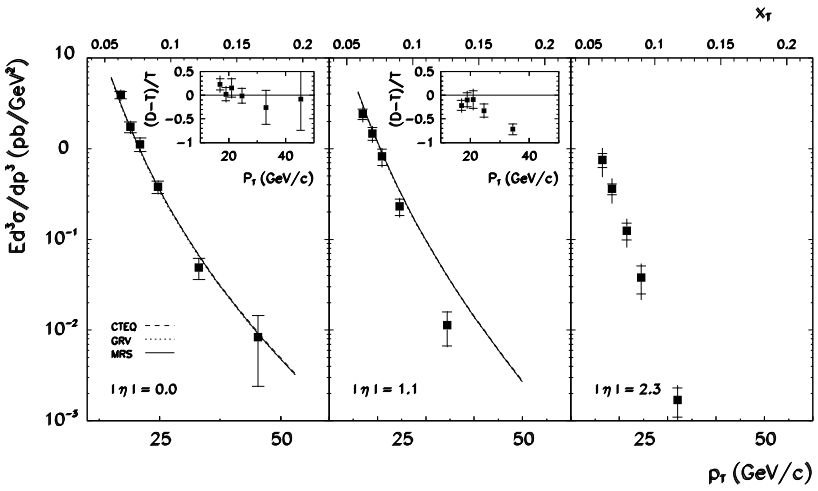

Figure 13. The UA1 546 GeV (cm energy) proton–antiproton prompt photon p_T distribution. The theoretical predictions are displayed for the two lower-η data sets, together with the $(D - T)/T$ comparisons in the insets. The $\eta = 2.3$ data fall outside the range of validity of the approximation made in the theoretical calculation of the isolated cross section.

Table 13. The invariant cross section for single prompt photon production in proton–antiproton collisions at a centre-of-mass energy of 630 GeV, as a function of the photon's transverse momentum, in three pseudorapidity regions, $\eta = 0.0$, 1.1, and 2.3, as measured by the CERN UA1 experiment. These data are produced using a photon isolation cut as described in the introduction. There is also an additional 23% overall systematic uncertainty.

CERN UA1	$\bar{\text{p}}\ \text{p} \rightarrow \gamma\ \text{X}$	$\sqrt{s} = 630$ GeV
Albajar *et al* 1988		*Phys. Lett.* **209B** 385

$\lvert\eta\rvert$	p_T^{mid} (GeV/c)	x_T^{mid}	$E\text{d}^3\sigma/\text{d}p^3$ (pb/GeV^2)
0.0	17.00	0.054	6.42 ± 0.57 ± 1.12
(−0.8–0.8)	19.00	0.060	3.30 ± 0.33 ± 0.52
	21.00	0.067	1.54 ± 0.20 ± 0.22
	23.00	0.073	0.74 ± 0.07 ± 0.09
	25.00	0.079	0.50 ± 0.05 ± 0.06
	27.00	0.086	0.381 ± 0.047 ± 0.038
	29.00	0.092	0.246 ± 0.037 ± 0.022
	31.50	0.100	0.123 ± 0.021 ± 0.010
	34.50	0.110	0.056 ± 0.014 ± 0.004
	37.50	0.119	0.051 ± 0.013 ± 0.003
	40.50	0.129	0.030 ± 0.010 ± 0.002
	46.00	0.146	0.0111 ± 0.0035 ± 0.0004
	55.00	0.175	0.0039 ± 0.0018 ± 0.0001
	65.00	0.206	0.0037 ± 0.0016 ± 0.0000
	75.00	0.238	0.0013 ± 0.0009 ± 0.0000
	90.00	0.286	0.0002 ± 0.0002 ± 0.0000
1.1	17.00	0.054	3.98 ± 0.49 ± 0.73
(0.8–1.4)	19.00	0.060	1.97 ± 0.27 ± 0.34
	21.00	0.067	1.00 ± 0.13 ± 0.17
	23.00	0.073	0.52 ± 0.06 ± 0.09
	25.00	0.079	0.397 ± 0.049 ± 0.065
	27.00	0.086	0.201 ± 0.034 ± 0.033
	31.00	0.098	0.073 ± 0.011 ± 0.012
	37.00	0.117	0.025 ± 0.006 ± 0.005
	45.00	0.143	0.0052 ± 0.0020 ± 0.0010
	60.00	0.190	0.0005 ± 0.0003 ± 0.0001
2.3	16.50	0.052	0.88 ± 0.07 ± 0.32
(1.6–3.0)	17.50	0.056	0.67 ± 0.06 ± 0.24
	18.50	0.059	0.47 ± 0.05 ± 0.17
	19.50	0.062	0.26 ± 0.03 ± 0.09
	20.50	0.065	0.20 ± 0.03 ± 0.07
	21.50	0.068	0.151 ± 0.024 ± 0.052
	22.50	0.071	0.115 ± 0.020 ± 0.040
	23.50	0.075	0.053 ± 0.013 ± 0.018
	24.50	0.078	0.050 ± 0.012 ± 0.017
	25.50	0.081	0.020 ± 0.008 ± 0.007
	28.00	0.089	0.0098 ± 0.0024 ± 0.0035
	32.00	0.102	0.0028 ± 0.0011 ± 0.0011
	37.00	0.117	0.0003 ± 0.0002 ± 0.0001

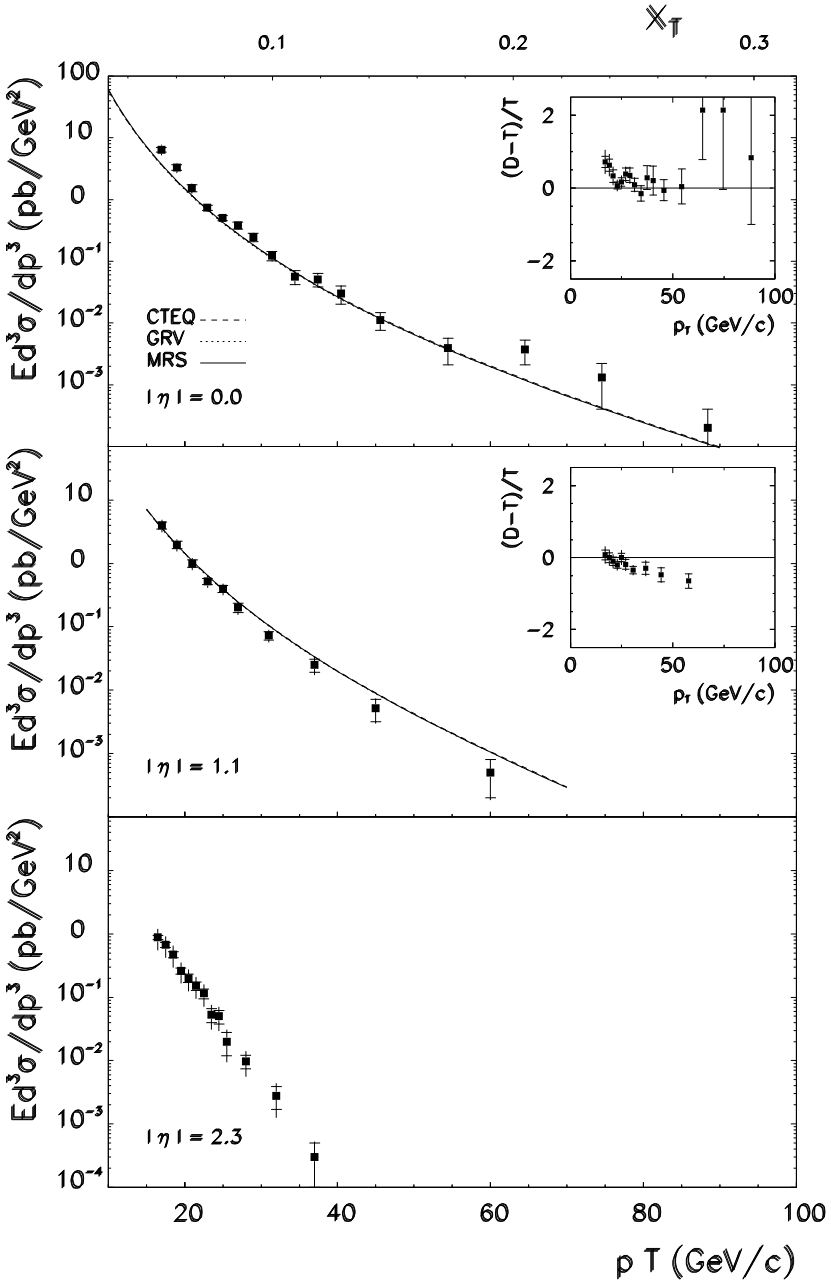

Figure 14. The UA1 630 GeV (cm energy) proton–antiproton prompt photon p_T distribution. The theoretical predictions are displayed for the two lower-η data sets, together with the $(D-T)/T$ comparisons in the insets. The $\eta = 2.3$ data fall outside the range of validity of the approximation made in the theoretical calculation of the isolated cross section.

Table 14. The invariant cross section for single prompt photon production in proton-antiproton collisions at a centre-of-mass energy of 630 GeV, as a function of the photon's transverse momentum, at $\eta = 1.4$, as measured by the CERN UA2 experiment. These data are produced using a photon isolation cut as described in the introduction. There is also an additional 20% overall systematic uncertainty.

CERN UA2 Ansari *et al* 1988	$\bar{\mathrm{p}}\ \mathrm{p} \rightarrow \gamma\ \mathrm{X}$		$\sqrt{s} = 630.00$ GeV *Z. Phys.* C **41** 395
$\lvert\eta\rvert$	p_T^{mid} (GeV/c)	x_T^{mid}	$E\mathrm{d}^3\sigma/\mathrm{d}p^3$ (pb/GeV^2)
1.4	13.00	0.041	9.4 ± 3.2
(1.0–1.8)	15.00	0.048	6.4 ± 1.5
	17.00	0.054	3.1 ± 0.8
	19.70	0.063	0.99 ± 0.30
	23.70	0.075	0.30 ± 0.12
	27.80	0.088	0.19 ± 0.07
	33.00	0.105	0.047 ± 0.024
	43.70	0.139	0.005 ± 0.004

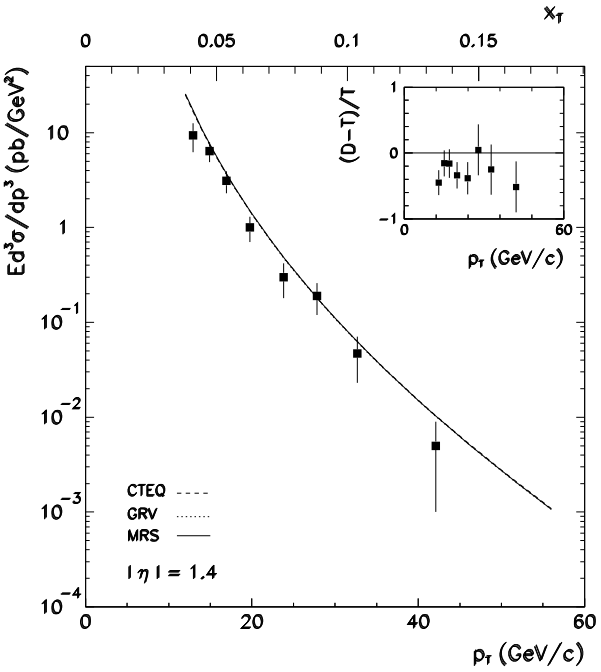

Figure 15. The UA2 630 GeV (cm energy) proton–antiproton prompt photon p_T distribution at $\eta = 1.4$. The theoretical predictions are displayed together with the $(D - T)/T$ comparison in the inset.

Table 15. The invariant cross section for single prompt photon production in proton–antiproton collisions at a centre-of-mass energy of 630 GeV, as a function of the photon's transverse momentum, at $\eta = 0.0$, as measured by the CERN UA2 experiment. These data are produced using a photon isolation cut as described in the introduction. There is also an additional 9% overall systematic uncertainty.

CERN UA2 Allitti *et al* 1992		$\bar{p}\,p \to \gamma\,X$			$\sqrt{s} = 630$ GeV *Phys. Lett.* **288B** 386
$\lvert\eta\rvert$	$\langle p_T \rangle$ (GeV/c)	$\langle x_T \rangle$	$E\mathrm{d}^3\sigma/\mathrm{d}p^3$ (pb/GeV^2)		
0.0	15.9	0.050	7.46	$\pm$ 0.410	$\pm$ 1.41
(−0.76–0.76)	17.9	0.057	3.97	$\pm$ 0.251	$\pm$ 0.671
	19.9	0.063	1.79	$\pm$ 0.156	$\pm$ 0.299
	21.9	0.070	0.992	$\pm$ 0.0713	$\pm$ 0.159
	23.9	0.076	0.615	$\pm$ 0.0500	$\pm$ 0.0793
	25.9	0.082	0.366	$\pm$ 0.0362	$\pm$ 0.0451
	28.7	0.091	0.151	$\pm$ 0.0160	$\pm$ 0.0182
	33.5	0.106	0.0657	$\pm$ 0.00728	$\pm$ 0.00769
	38.6	0.123	0.0179	$\pm$ 0.00367	$\pm$ 0.00168
	46.3	0.147	0.00694	$\pm$ 0.00171	$\pm$ 0.000750
	54.1	0.172	0.00231	$\pm$ 0.000936	$\pm$ 0.000349
	64.5	0.205	0.000484	$\pm$ 0.000272	$\pm$ 0.0000576
	82.3	0.261	0.000151	$\pm$ 0.0000999	$\pm$ 0.0000145

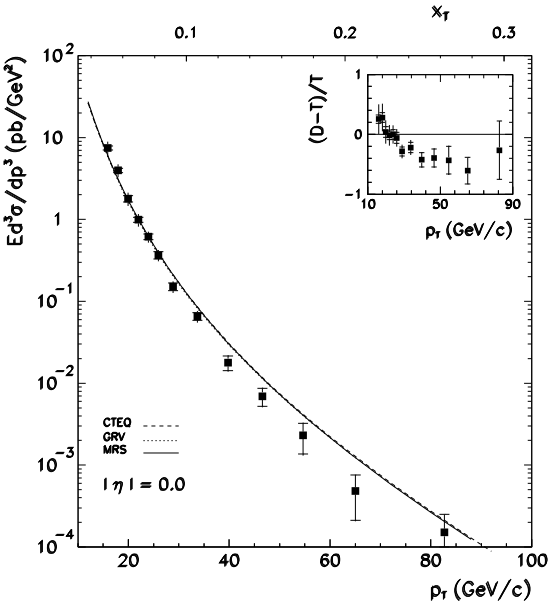

Figure 16. The UA2 630 GeV (cm energy) proton–antiproton prompt photon p_T distribution at $\eta = 0.0$. The theoretical predictions are displayed together with the $(D - T)/T$ comparison in the inset.

Table 16. Cross section for single prompt photon production in proton–antiproton collisions at a centre-of-mass energy of 1800 GeV, as a function of the photon's transverse momentum, in the region $|\eta| < 0.9$, as measured by the Fermilab E741(CDF) experiment. These data are produced using a photon isolation cut as described in the introduction. The systematic uncertainties given as percentages in the final column are the linear sum of the p_T dependent systematic errors and the approximately 10% normalization uncertainty.

FNAL E741(CDF) Abe *et al* 1994	$\bar{p}\ p \to \gamma\ X$		$\sqrt{s} = 1800$ GeV *Phys. Rev. Lett.* **73** 2662
$\lvert\eta\rvert$	$\langle p_T \rangle$ (GeV/c)	$\langle x_T \rangle$	$d^2\sigma/dp_T/d\eta$ (pb/GeV)
< 0.9	12.3	0.014	4460.0 ± 415.0 ± 16%
	17.0	0.019	1300.0 ± 38.0 ± 12%
	19.0	0.021	805.0 ± 21.0 ± 11%
	21.0	0.023	458.0 ± 15.0 ± 10%
	23.0	0.026	308.0 ± 12.0 ± 10%
	25.0	0.028	226.0 ± 10.0 ± 10%
	27.0	0.030	163.0 ± 8.0 ± 10%
	29.0	0.032	106.0 ± 6.0 ± 10%
	31.0	0.034	76.7 ± 5.5 ± 9%
	33.9	0.038	53.7 ± 3.2 ± 9%
	37.9	0.042	30.9 ± 2.4 ± 9%
	41.9	0.047	20.5 ± 1.9 ± 9%
	48.9	0.054	7.61 ± 0.76 ± 10%
	62.4	0.069	3.09 ± 0.32 ± 10%
	80.8	0.090	0.911 ± 0.159 ± 10%
	114.7	0.127	0.163 ± 0.041 ± 11%

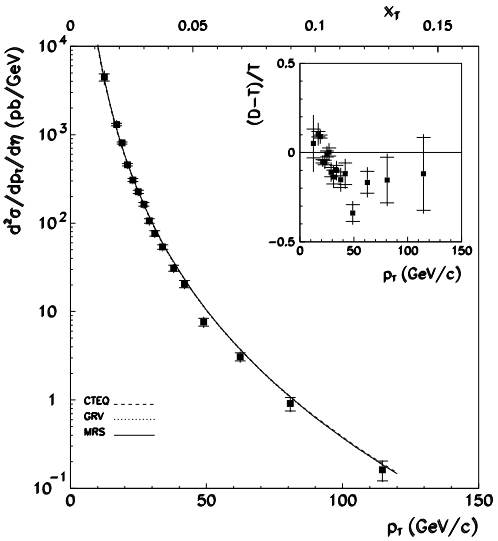

Figure 17. The CDF 1800 GeV (cm energy) proton–antiproton prompt photon p_T distribution. The theoretical predictions are displayed together with the $(D - T)/T$ comparison in the inset.

Table 17. The invariant cross section for single prompt photon production in proton–antiproton collisions at a centre-of-mass energy of 1800 GeV, as a function of the photon's transverse momentum, in the region $|\eta| < 0.9$, as measured by the Fermilab E740(D0) experiment. These data are produced using a photon isolation cut as described in the introduction. The systematic error is shown as a percentage in the final column. Note that this contains a large part (5.4%) p_T correlated normalization uncertainty.

FNAL E740(D0) Abachi *et al* 1996		$\bar{p}\ p \rightarrow \gamma\ X$		$\sqrt{s} = 1800$ GeV *Phys. Rev. Lett.* **77** 5011
$\lvert\eta\rvert$	$\langle E_T \rangle$ (GeV)	$\langle x_T \rangle$	$d^2\sigma/dE_T/d\eta$ (pb/GeV)	
< 0.9	10.5	0.012	14200.0 ± 291.0	± 73.0%
	13.5	0.015	4010.0 ± 153.0	± 42.0%
	16.5	0.018	1290.0 ± 89.7	± 24.0%
	19.5	0.022	661.0 ± 67.1	± 19.0%
	22.5	0.025	315.0 ± 15.2	± 14.0%
	25.5	0.028	157.0 ± 11.0	± 12.0%
	28.5	0.032	105.0 ± 9.31	± 11.0%
	31.5	0.035	63.9 ± 7.53	± 10.0%
	37.4	0.042	28.1 ± 0.551	± 8.6%
	40.5	0.045	19.7 ± 0.466	± 8.6%
	43.5	0.048	14.2 ± 0.404	± 8.6%
	46.5	0.052	11.1 ± 0.366	± 8.6%
	49.5	0.055	7.76 ± 0.312	± 8.6%
	52.5	0.058	5.83 ± 0.276	± 8.6%
	55.5	0.062	4.72 ± 0.253	± 8.6%
	58.5	0.065	3.30 ± 0.215	± 8.6%
	61.5	0.068	2.98 ± 0.207	± 8.6%
	65.7	0.073	2.17 ± 0.13	± 8.6%
	72.0	0.080	1.39 ± 0.10	± 8.6%
	78.0	0.087	0.88 ± 0.08	± 8.6%
	85.1	0.095	0.67 ± 0.06	± 10.0%
	94.4	0.105	0.28 ± 0.04	± 14.0%
	108.4	0.120	0.11 ± 0.02	± 18.0%

Table 18. The invariant cross section for single prompt photon production in proton–antiproton collisions at a centre-of-mass energy of 1800 GeV, as a function of the photon's transverse momentum, in the region $1.6 < |\eta| < 2.5$, as measured by the Fermilab E740(D0) experiment. These data are produced using a photon isolation cut as described in the introduction. The systematic error is shown as a percentage in the final column. Note that this contains a large part (5.4%) p_T correlated normalization uncertainty.

FNAL E740(D0) Abachi *et al* 1996		$\bar{p}\ p \rightarrow \gamma\ X$		$\sqrt{s} = 1800$ GeV *Phys. Rev. Lett.* **77** 5011
$\lvert\eta\rvert$	$\langle E_T \rangle$ (GeV)	$\langle x_T \rangle$	$d^2\sigma/dE_T/d\eta$ (pb/GeV)	
1.6–2.5	10.5	0.012	10300.0 ± 250.0	± 72.0%
	13.5	0.015	2840.0 ± 131.0	± 43.0%
	16.5	0.018	1130.0 ± 86.3	± 35.0%
	19.5	0.022	468.0 ± 58.5	± 24.0%
	22.5	0.025	227.0 ± 13.2	± 20.0%
	25.5	0.028	126.0 ± 10.2	± 17.0%
	28.5	0.032	66.0 ± 7.62	± 17.0%
	31.5	0.035	43.3 ± 6.39	± 17.0%
	37.5	0.042	19.4 ± 0.458	± 17.0%
	40.5	0.045	13.0 ± 0.386	± 17.0%
	43.5	0.048	9.04 ± 0.329	± 17.0%
	46.5	0.052	6.60 ± 0.287	± 17.0%
	49.5	0.055	4.80 ± 0.250	± 17.0%
	52.5	0.058	3.01 ± 0.202	± 17.0%
	55.5	0.062	2.66 ± 0.193	± 17.0%
	58.5	0.065	1.59 ± 0.152	± 17.0%
	61.5	0.068	1.43 ± 0.146	± 17.0%
	65.8	0.073	0.85 ± 0.08	± 17.0%
	71.6	0.080	0.40 ± 0.06	± 17.0%
	77.9	0.087	0.31 ± 0.05	± 17.0%
	85.0	0.094	0.13 ± 0.03	± 18.0%
	94.7	0.105	0.09 ± 0.02	± 22.0%
	105.8	0.118	0.03 ± 0.01	± 26.0%

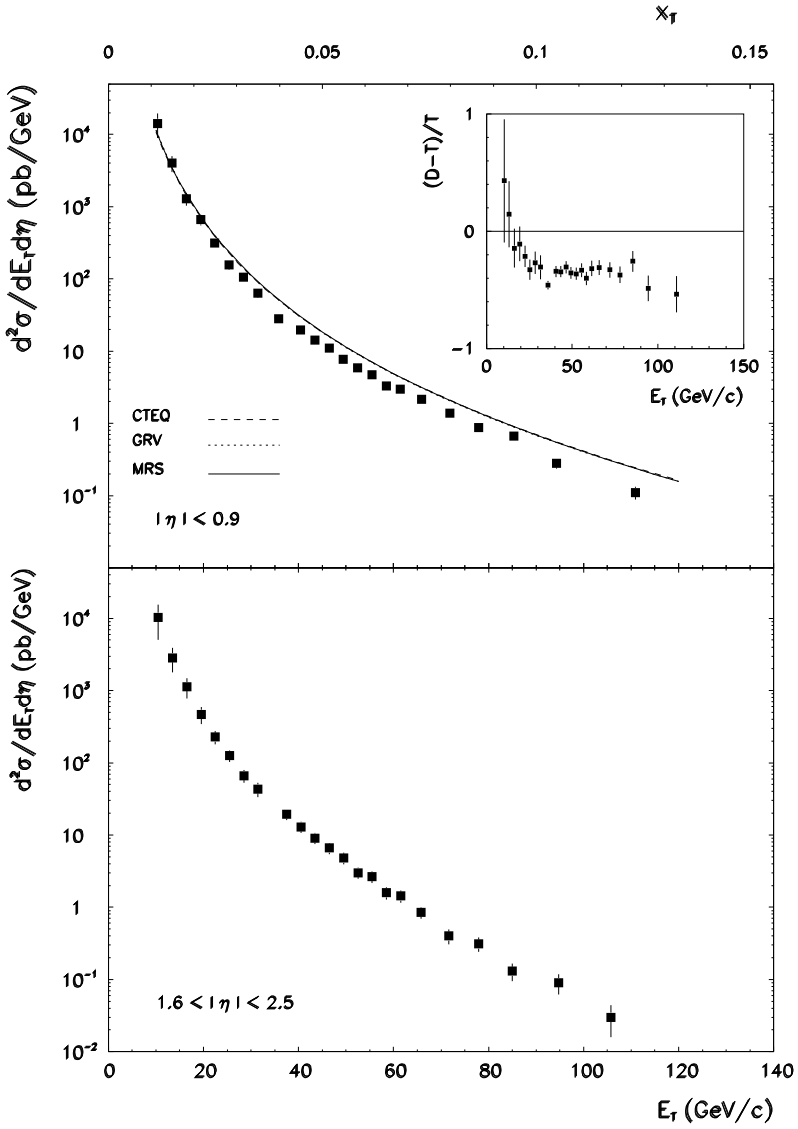

Figure 18. The E740(D0) 1800 GeV (cm energy) proton-antiproton prompt photon p_T distributions at $|\eta| < 0.9$ and $1.6 < |\eta| < 2.5$. The theoretical predictions are displayed, together with the $(D-T)/T$ comparison in the inset, for the $\eta = 0.0$ data set. The other data, taken in the forward region, fall outside the range of validity of the approximation made in the theoretical calculation of the isolated cross section.

Table 19. The invariant cross section for single prompt photon production in proton–carbon collisions at incident beam momentum 200 GeV/c, as a function of the photon's transverse momentum, in the region $-0.75 < y < 0.2$, as measured by the Fermilab E629 experiment. The errors include systematic uncertainties.

FNAL E629	p C → γ X	$\sqrt{s} = 19.40$ GeV
McLaughlin *et al* 1983		*Phys. Rev. Lett.* **51** 971

y	p_T (GeV/c)	$p_T^{\rm mid}$ (GeV/c)	$x_T^{\rm mid}$	$E{\rm d}^3\sigma/{\rm d}p^3$ (pb/GeV^2)
−0.75–0.2	2.1–2.4	2.25	0.232	<19000
	2.4–2.5	2.45	0.253	< 7600
	2.5–2.6	2.55	0.263	2400 ± 4700
	2.6–2.8	2.70	0.278	4600 ± 2300
	2.8–3.0	2.90	0.299	2700 ± 1100
	3.0–3.5	3.25	0.335	1100 ± 300
	3.5–4.0	3.75	0.387	160 ± 80
	4.0–5.0	4.50	0.464	58 ± 25

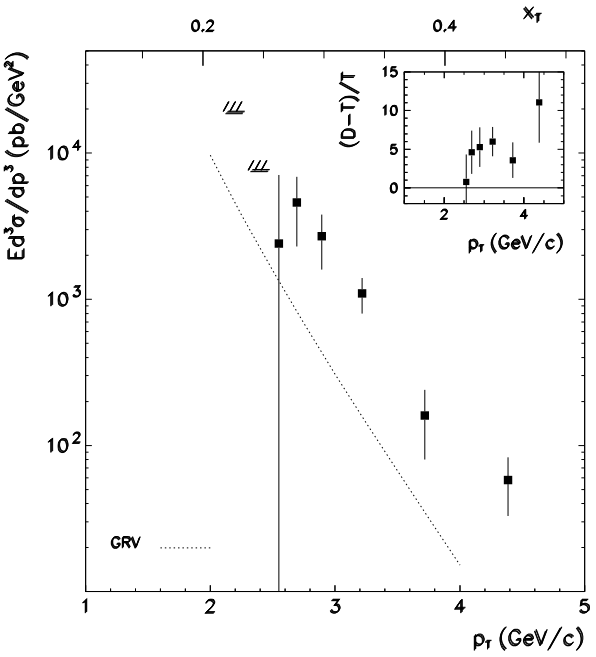

Figure 19. The E629 proton–carbon prompt photon p_T distribution. The theoretical prediction using the GRV94 structure function parametrisation is shown together with the $(D - T)/T$ comparison in the inset. The kinematical range in p_T is too low for the applicability of MRS or CTEQ sets.

Table 20. The invariant cross section for single prompt photon production in proton–carbon collisions at incident beam momentum 200 GeV/c, as a function of the photon's transverse momentum, in the region $-0.4 < y < 1.2$, as measured by the CERN NA3 experiment. Data are given for two different experimental conditions described as (a) the conversion trigger and (b) the calorimeter trigger. Additional systematic errors are ≈30% for (a) and ≈40% for (b)

CERN NA3	p C → γ X	$\sqrt{s} = 19.40$ GeV
Badier *et al* 1986		*Z. Phys.* C **31** 341

y	$\langle p_T \rangle$ (GeV/c)	$\langle x_T \rangle$	$E\mathrm{d}^3\sigma/\mathrm{d}p^3$ (pb/GeV^2)
(a)			
−0.4–1.2	2.94	0.303	21800.0 ± 4320.0
	3.09	0.319	7630.0 ± 1780.0
	3.33	0.343	3640.0 ± 730.0
	3.70	0.381	980.0 ± 220.0
	4.21	0.434	160.0 ± 66.0
	4.98	0.513	15.0 ± 8.3
(b)			
−0.4–0.8	3.90	0.402	620.0 ± 190.0
	4.10	0.423	440.0 ± 110.0
	4.30	0.443	270.0 ± 70.0
	4.50	0.464	110.0 ± 40.0
	4.70	0.485	45.0 ± 29.0
	5.00	0.515	47.0 ± 13.0

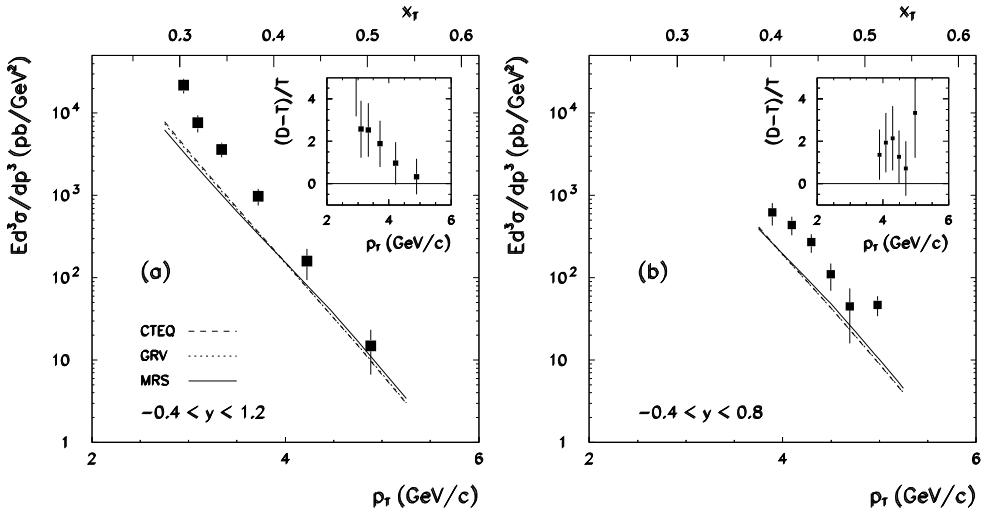

Figure 20. The NA3 proton–carbon prompt photon p_T distributions. The theoretical predictions are displayed together with the $(D - T)/T$ comparisons in the insets.

Table 21. The invariant cross section for single prompt photon production in proton–beryllium collisions at incident beam momentum 500 GeV/c, as a function of the photon's transverse momentum, in four y ranges from −0.7 to 0.7, as measured by the Fermilab E706 experiment.

FNAL E706 Alverson *et al* 1993	p Be → γ X			$\sqrt{s} = 30.63$ GeV *Phys. Rev.* D **48** 5
y	p_T (GeV/c)	p_T^{mid} (GeV/c)	x_T^{mid}	$E\mathrm{d}^3\sigma/\mathrm{d}p^3$ (pb/GeV^2)
−0.7 – −0.2	4.0 –4.5	4.25	0.278	134.0 ± 34.0 ± 50.0
	4.5 –5.0	4.75	0.310	54.0 ± 12.0 ± 14.0
	5.0 –6.0	5.50	0.359	6.3 ± 2.7 ± 1.5
	6.0 –7.0	6.50	0.424	0.97 ± 0.64 ± 0.19
−0.2 – 0.2	4.0 –4.5	4.25	0.278	161.0 ± 34.0 ± 38.0
	4.5 –5.0	4.75	0.310	65.0 ± 12.0 ± 14.0
	5.0 –6.0	5.50	0.359	6.6 ± 3.1 ± 1.8
	6.0 –7.0	6.50	0.424	2.4 ± 0.9 ± 0.5
0.2 – 0.7	4.0 –4.5	4.25	0.278	139.0 ± 26.0 ± 33.0
	4.5 –5.0	4.75	0.310	37.0 ± 10.0 ± 9.0
	5.0 –6.0	5.50	0.359	7.4 ± 2.5 ± 1.7
	6.0 –7.0	6.50	0.424	0.86 ± 0.69 ± 0.20
−0.7 – 0.7	4.0 –4.25	4.125	0.269	190.0 ± 30.0 ± 46.0
	4.25–4.5	4.325	0.282	103.0 ± 20.0 ± 23.0
	4.5 –4.75	4.625	0.302	66.0 ± 11.0 ± 15.0
	4.75–5.0	4.825	0.318	36.0 ± 7.0 ± 8.0
	5.0 –5.5	5.25	0.343	6.8 ± 2.7 ± 1.9
	5.5 –6.0	5.75	0.375	6.5 ± 1.6 ± 1.3
	6.0 –7.0	6.50	0.424	1.32 ± 0.43 ± 0.25
	7.0 –8.0	7.50	0.490	0.06 ± 0.08 ± 0.01

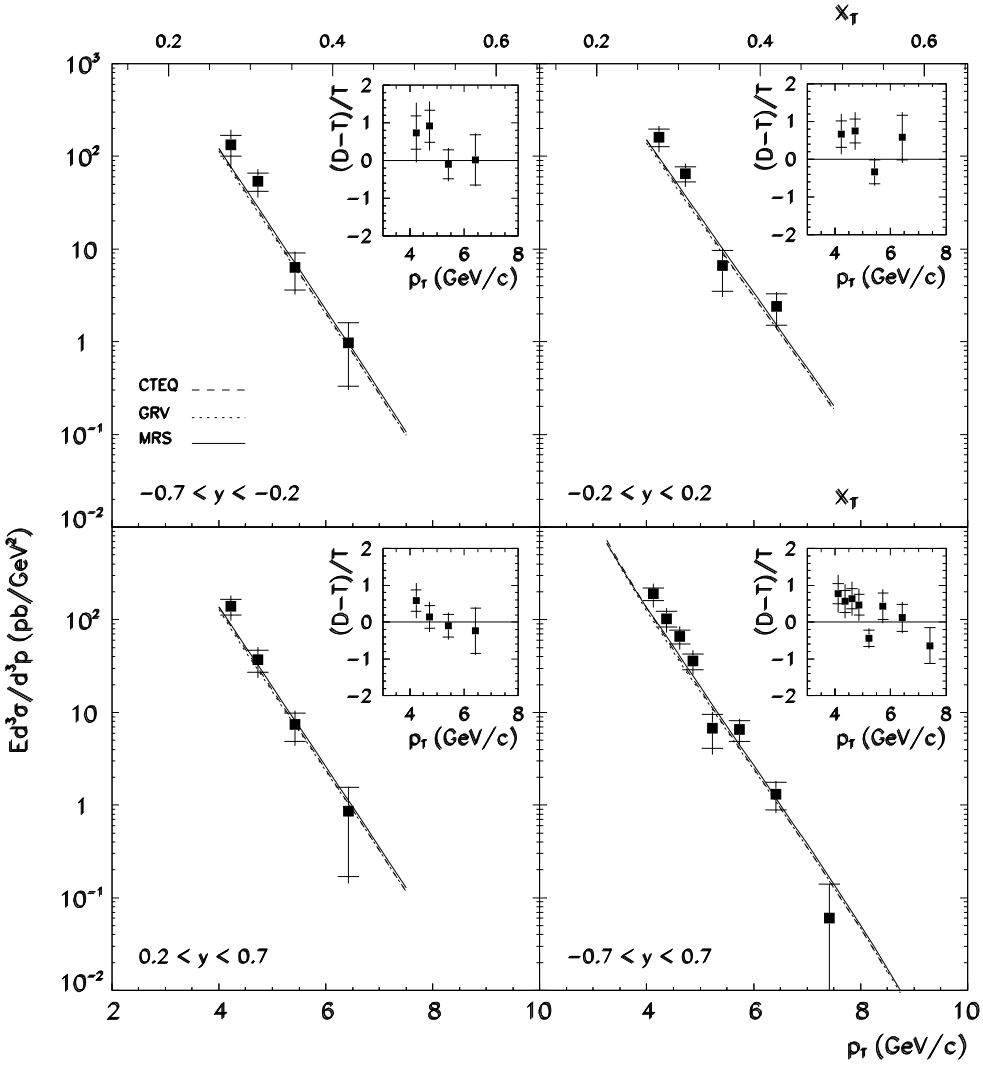

Figure 21. The E706 proton–beryllium prompt photon p_T distributions. The theoretical predictions are displayed together with the $(D-T)/T$ comparisons in the insets.

Table 22. The invariant cross section for single prompt photon production in π^+–proton collisions at incident beam momentum 280 GeV/c, as a function of the photon's transverse momentum, in five x_F regions from −0.45 to 0.55, as measured by the CERN WA70 experiment.

CERN WA70	π^+ p $\to \gamma$ X	$\sqrt{s} = 22.94$ GeV
Bonesini *et al* 1988		*Z. Phys.* C **37** 535

x_F	p_T (GeV/c)	$\langle p_T \rangle$ (GeV/c)	$\langle x_T \rangle$	$E\mathrm{d}^3\sigma/\mathrm{d}p^3$ (pb/GeV^2)
−0.45 – −0.25	4.00–4.25	4.11	0.358	19.3 ± 7.2 ± 7.4
	4.25–4.50	4.36	0.380	11.4 ± 4.6 ± 3.9
	4.50–4.75	4.61	0.402	11.0 ± 3.6 ± 2.6
	4.75–5.00	4.86	0.424	6.6 ± 2.6 ± 1.3
	5.00–5.50	5.21	0.454	1.8 ± 0.9 ± 0.4
−0.25 – −0.05	4.00–4.25	4.11	0.358	47.3 ± 7.1 ± 10.3
	4.25–4.50	4.36	0.380	40.4 ± 5.7 ± 6.9
	4.50–4.75	4.61	0.402	18.8 ± 3.7 ± 3.1
	4.75–5.00	4.86	0.424	9.8 ± 2.8 ± 1.7
	5.00–5.50	5.21	0.454	5.5 ± 1.4 ± 0.8
	5.50–6.00	5.71	0.498	2.2 ± 0.8 ± 0.3
	6.00–7.00	6.34	0.553	0.8 ± 0.3 ± 0.1
−0.05 – 0.15	4.00–4.25	4.11	0.358	44.0 ± 7.1 ± 10.2
	4.25–4.50	4.36	0.380	35.7 ± 6.0 ± 6.9
	4.50–4.75	4.61	0.402	18.5 ± 4.1 ± 3.7
	4.75–5.00	4.86	0.424	17.8 ± 3.5 ± 2.7
	5.00–5.50	5.21	0.454	8.0 ± 1.6 ± 1.1
	5.50–6.00	5.71	0.498	2.3 ± 0.9 ± 0.3
	6.00–7.00	6.34	0.553	0.4 ± 0.2 ± 0.1
0.15 – 0.35	4.00–4.25	4.11	0.358	51.3 ± 8.7 ± 11.6
	4.25–4.50	4.36	0.380	28.2 ± 6.0 ± 5.5
	4.50–4.75	4.61	0.402	17.5 ± 4.5 ± 3.5
	4.75–5.00	4.86	0.424	5.8 ± 2.8 ± 1.4
	5.00–5.50	5.21	0.454	5.6 ± 1.6 ± 0.9
	5.50–6.00	5.71	0.498	0.6 ± 0.5 ± 0.1
	6.00–7.00	6.34	0.553	0.5 ± 0.3 ± 0.1
0.35 – 0.55	4.00–4.25	4.11	0.358	22.3 ± 9.5 ± 9.9
	4.25–4.50	4.36	0.380	32.6 ± 7.5 ± 7.6
	4.50–4.75	4.61	0.402	10.4 ± 4.9 ± 3.4
	4.75–5.00	4.86	0.424	2.9 ± 2.7 ± 1.5
	5.00–5.50	5.21	0.454	3.6 ± 1.7 ± 0.9

Table 23. The invariant cross section for single prompt photon production in π^+–proton collisions at incident beam momentum 280 GeV/c, as a function of the photon's transverse momentum, in four x_F regions from -0.45 to 0.45, as measured by the CERN WA70 experiment.

CERN WA70	$\pi^+ \text{ p} \rightarrow \gamma \text{ X}$	$\sqrt{s} = 22.94$ GeV
Bonesini *et al* 1988		*Z. Phys.* C **37** 535

x_F	p_T (GeV/c)	$\langle p_T \rangle$ (GeV/c)	$\langle x_T \rangle$	$E\mathrm{d}^3\sigma/\mathrm{d}p^3$ (pb/GeV^2)
−0.45 – −0.15	4.00–4.25	4.11	0.358	24.45 ± 5.33 ± 6.93
	4.25–4.50	4.36	0.380	21.58 ± 3.90 ± 4.41
	4.50–4.75	4.61	0.402	11.47 ± 2.72 ± 2.33
	4.75–5.00	4.86	0.424	5.65 ± 1.97 ± 1.11
	5.00–5.50	5.21	0.454	3.16 ± 0.91 ± 0.49
	5.50–6.00	5.71	0.498	1.07 ± 0.49 ± 0.18
	6.00–6.50	6.21	0.541	0.54 ± 0.32 ± 0.14
−0.15 – 0.15	4.00–4.25	4.11	0.358	49.07 ± 5.90 ± 10.34
	4.25–4.50	4.36	0.380	37.63 ± 4.86 ± 6.69
	4.50–4.75	4.61	0.402	20.39 ± 3.30 ± 3.39
	4.75–5.00	4.86	0.424	16.71 ± 2.75 ± 2.46
	5.00–5.50	5.21	0.454	7.03 ± 1.23 ± 1.00
	5.50–6.00	5.71	0.498	2.06 ± 0.66 ± 0.29
	6.00–6.50	6.21	0.541	0.65 ± 0.36 ± 0.12
0.15 – 0.45	4.00–4.25	4.11	0.358	45.69 ± 6.89 ± 9.97
	4.25–4.50	4.36	0.380	25.41 ± 4.84 ± 4.83
	4.50–4.75	4.61	0.402	15.98 ± 3.60 ± 2.96
	4.75–5.00	4.86	0.424	4.91 ± 2.25 ± 1.21
	5.00–5.50	5.21	0.454	5.51 ± 1.33 ± 0.82
	5.50–6.00	5.71	0.498	0.42 ± 0.42 ± 0.12
	6.00–6.50	6.21	0.541	0.55 ± 0.38 ± 0.10
−0.45 – 0.45	4.00–4.25	4.11	0.358	38.20 ± 3.36 ± 7.97
	4.25–4.50	4.36	0.380	28.42 ± 2.61 ± 4.98
	4.50–4.75	4.61	0.402	16.07 ± 1.84 ± 2.65
	4.75–5.00	4.86	0.424	9.37 ± 1.35 ± 1.52
	5.00–5.50	5.21	0.454	5.25 ± 0.66 ± 0.82
	5.50–6.00	5.71	0.498	1.25 ± 0.32 ± 0.20
	6.00–6.50	6.21	0.541	0.59 ± 0.20 ± 0.11
	6.50–7.00	6.71	0.585	0.40 ± 0.16 ± 0.08

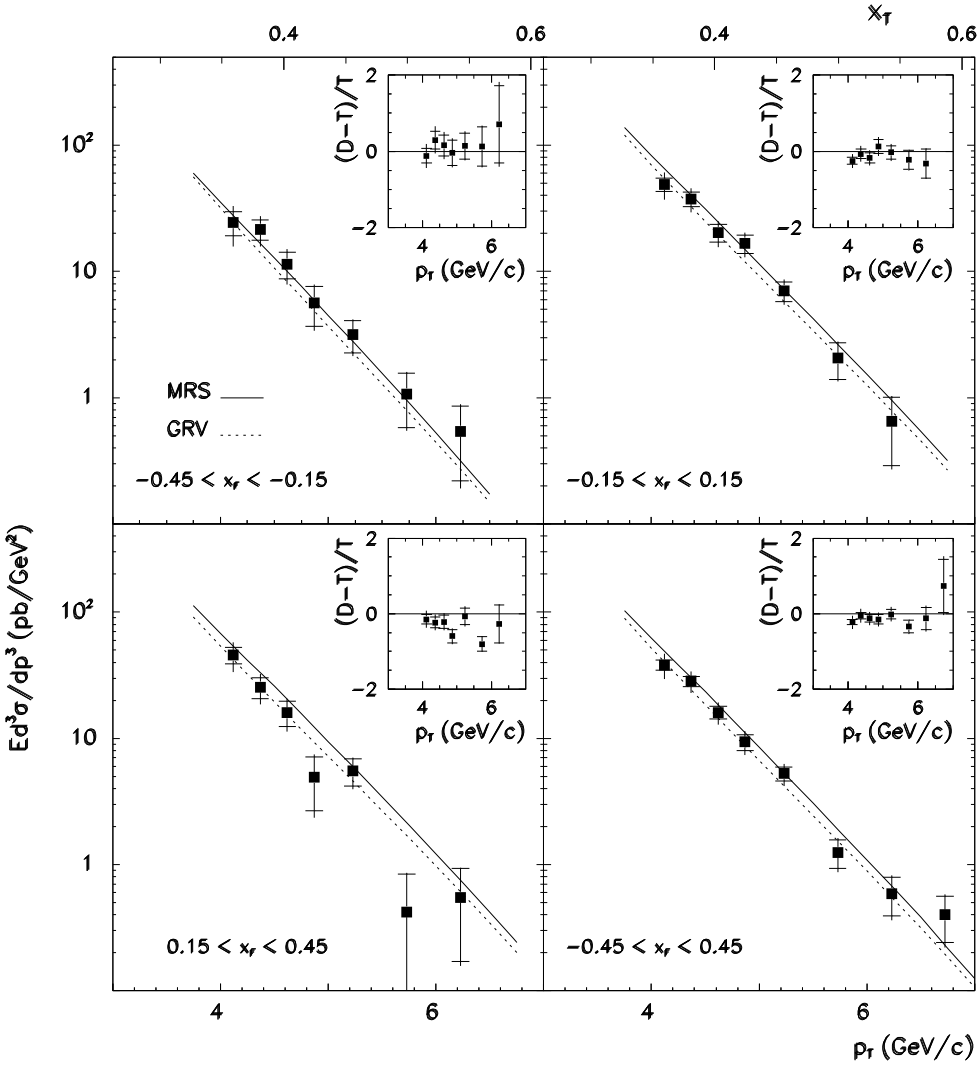

Figure 22. The WA70 π^+–proton prompt photon p_T distributions in the wider x_F bins. The theoretical predictions are displayed together with the $(D - T)/T$ comparisons in the insets.

Table 24. The invariant cross section for single prompt photon production in π^+–proton collisions at incident beam momentum 280 GeV/c, as a function of x_F, in two p_T regions from 4 to 6 GeV/c, as measured by the CERN WA70 experiment.

CERN WA70	$\pi^+ \, p \to \gamma \, X$	$\sqrt{s} = 22.94$ GeV
Bonesini *et al* 1988		*Z. Phys.* C **37** 535

p_T (GeV/c)	x_F	$x_F^{\rm mid}$	$E{\rm d}^3\sigma/{\rm d}p^3$ (pb/GeV^2)
4.0–5.0	−0.45 – −0.35	−0.40	10.88 ± 3.89 ± 2.92
	−0.35 – −0.25	−0.30	14.47 ± 3.24 ± 3.33
	−0.25 – −0.15	−0.20	24.43 ± 3.44 ± 4.44
	−0.15 – −0.05	−0.10	35.26 ± 3.73 ± 5.79
	−0.05 – 0.05	0.00	29.79 ± 3.65 ± 5.28
	0.05 – 0.15	0.10	30.39 ± 4.00 ± 5.59
	0.15 – 0.25	0.20	29.34 ± 4.21 ± 5.39
	0.25 – 0.35	0.30	21.96 ± 3.98 ± 4.40
	0.35 – 0.45	0.40	14.57 ± 4.00 ± 4.07
	0.45 – 0.55	0.50	14.31 ± 5.43 ± 5.51
5.0–6.0	−0.45 – −0.35	−0.40	1.43 ± 0.85 ± 0.31
	−0.35 – −0.25	−0.30	0.89 ± 0.68 ± 0.23
	−0.25 – −0.15	−0.20	4.29 ± 1.18 ± 0.64
	−0.15 – −0.05	−0.10	3.29 ± 1.09 ± 0.52
	−0.05 – 0.05	0.00	5.01 ± 1.25 ± 0.73
	0.05 – 0.15	0.10	5.51 ± 1.31 ± 0.79
	0.15 – 0.25	0.20	4.55 ± 1.31 ± 0.67
	0.25 – 0.35	0.30	1.45 ± 0.93 ± 0.33
	0.35 – 0.45	0.40	2.55 ± 1.28 ± 0.60
	0.45 – 0.55	0.50	0.49 ± 1.21 ± 0.63

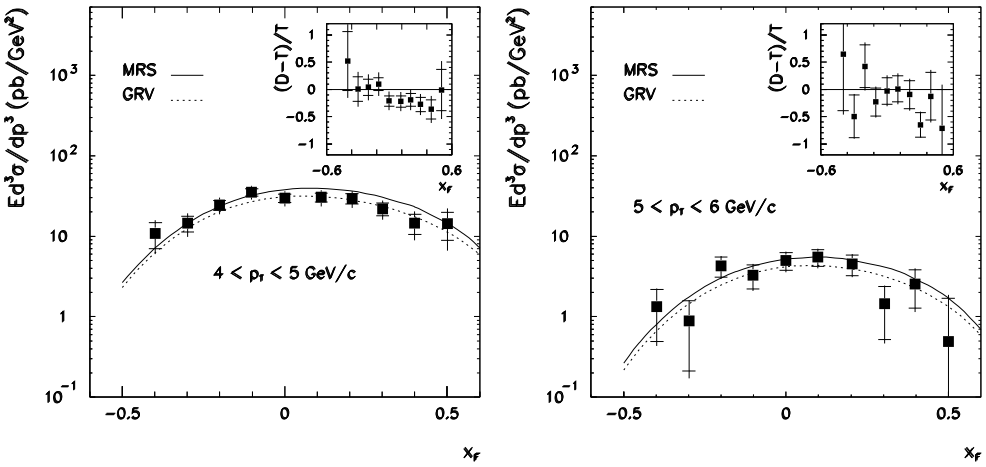

Figure 23. The WA70 π^+–proton prompt photon x_F distributions. The theoretical predictions are displayed together with the $(D-T)/T$ comparisons in the insets.

Table 25. The invariant cross section for single prompt photon production in π^+–proton collisions at incident beam momentum 300 GeV/c, as a function of the photon's transverse momentum, in the region $-0.65 < y < 0.52$, as measured by the CERN NA24 experiment. There is an additional 7% uncertainty in the normalization.

CERN NA24	π^+ p $\to \gamma$ X	$\sqrt{s} = 23.75$ GeV
De Marzo *et al* 1987		*Phys. Rev.* D **36** 8

y	p_T (GeV/c)	$p_T^{\rm mid}$ (GeV/c)	$x_T^{\rm mid}$	$E{\rm d}^3\sigma/{\rm d}p^3$ (pb/GeV^2)
−0.65–0.52	3.0–3.5	3.25	0.274	772.0 ± 150.0 ± 160.0
	3.5–4.0	3.75	0.316	310.0 ± 76.0 ± 39.0
	4.0–4.5	4.25	0.358	54.2 ± 8.7 ± 7.9
	4.5–5.5	5.00	0.421	10.00 ± 2.50 ± 2.50
	5.5–6.5	6.00	0.505	0.831 ± 0.570 ± 0.120

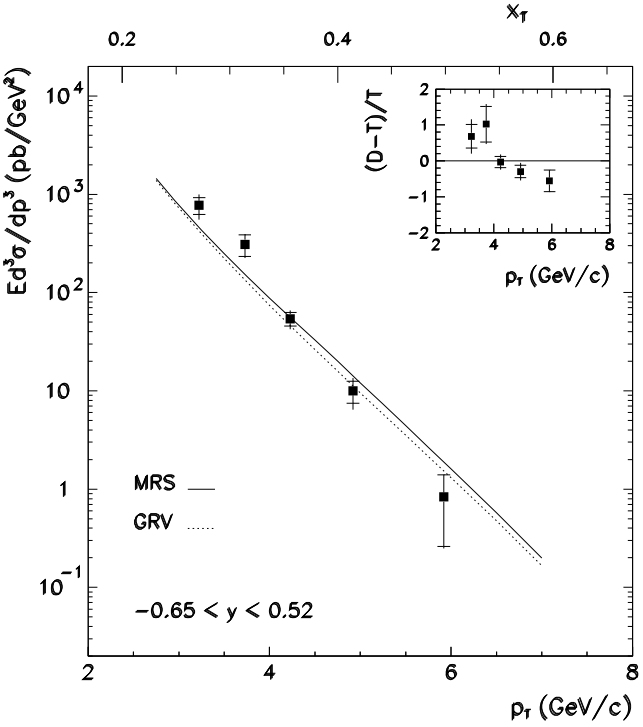

Figure 24. The NA24 π^+–proton prompt photon p_T distribution. The theoretical predictions are displayed together with the $(D - T)/T$ comparison in the inset.

Table 26. The invariant cross section for single prompt photon production in π^-–proton collisions at incident beam momentum 280 GeV/c, as a function of the photon's transverse momentum, in 10 x_F regions from −0.45 to 0.55, as measured by the CERN WA70 experiment.

CERN WA70 Bonesini *et al* 1988	π^- p $\rightarrow \gamma$ X			$\sqrt{s} = 22.94$ GeV *Z. Phys.* C **37** 535
x_F	p_T (GeV/c)	$\langle p_T \rangle$ (GeV/c)	$\langle x_T \rangle$	$E\mathrm{d}^3\sigma/\mathrm{d}p^3$ (pb/GeV^2)
−0.45 – −0.35	4.00–4.25	4.12	0.389	10.7 ± 10.6 ± 7.2
	4.25–4.50	4.37	0.381	27.9 ± 7.6 ± 9.9
	4.50–4.75	4.62	0.403	8.0 ± 3.3 ± 2.8
	4.75–5.00	4.87	0.425	7.7 ± 2.6 ± 2.3
	5.00–5.50	5.21	0.454	1.7 ± 1.1 ± 0.6
	5.50–6.00	5.71	0.498	2.0 ± 0.7 ± 0.5
−0.35 – −0.25	4.00–4.25	4.12	0.359	47.1 ± 6.5 ± 14.4
	4.25–4.50	4.37	0.381	35.0 ± 4.9 ± 7.5
	4.50–4.75	4.62	0.403	19.9 ± 3.6 ± 4.9
	4.75–5.00	4.87	0.425	16.7 ± 2.8 ± 3.1
	5.00–5.50	5.21	0.454	4.3 ± 1.0 ± 0.9
	5.50–6.00	5.71	0.498	2.1 ± 0.6 ± 0.4
−0.25 – −0.15	4.00–4.25	4.12	0.359	75.7 ± 6.8 ± 16.8
	4.25–4.50	4.37	0.381	45.3 ± 4.7 ± 8.9
	4.50–4.75	4.62	0.403	33.9 ± 3.7 ± 5.9
	4.75–5.00	4.87	0.425	19.8 ± 2.9 ± 3.4
	5.00–5.50	5.21	0.454	9.7 ± 1.4 ± 1.6
	5.50–6.00	5.71	0.498	6.2 ± 1.0 ± 1.0
	6.00–7.00	6.36	0.554	1.19 ± 0.30 ± 0.22
−0.15 – −0.05	4.00–4.25	4.12	0.359	106.1 ± 7.3 ± 22.1
	4.25–4.50	4.37	0.381	73.5 ± 5.8 ± 13.2
	4.50–4.75	4.62	0.403	48.8 ± 4.3 ± 7.8
	4.75–5.00	4.87	0.425	23.0 ± 3.0 ± 3.9
	5.00–5.50	5.21	0.454	11.6 ± 1.5 ± 1.9
	5.50–6.00	5.71	0.498	5.0 ± 0.9 ± 0.8
	6.00–7.00	6.36	0.554	1.35 ± 0.32 ± 0.26
−0.05 – 0.05	4.00–4.25	4.12	0.359	103.1 ± 7.1 ± 21.2
	4.25–4.50	4.37	0.381	71.0 ± 5.9 ± 13.2
	4.50–4.75	4.62	0.403	45.7 ± 4.2 ± 7.5
	4.75–5.00	4.87	0.425	33.8 ± 3.5 ± 5.5
	5.00–5.50	5.21	0.454	15.4 ± 1.7 ± 2.4
	5.50–6.00	5.71	0.498	8.6 ± 1.2 ± 1.4
	6.00–7.00	6.36	0.554	1.51 ± 0.35 ± 0.27

Table 26. WA70 π^-–p continued.

CERN WA70 Bonesini *et al* 1988	π^- p $\to \gamma$ X			$\sqrt{s} = 22.94$ GeV *Z. Phys.* C **37** 535
x_F	p_T (GeV/c)	$\langle p_T \rangle$ (GeV/c)	$\langle x_T \rangle$	$E\mathrm{d}^3\sigma/\mathrm{d}p^3$ (pb/GeV^2)
0.05–0.15	4.00–4.25	4.12	0.359	117.5 ± 7.6 ± 23.9
	4.25–4.50	4.37	0.381	83.5 ± 6.5 ± 15.3
	4.50–4.75	4.62	0.403	48.4 ± 4.6 ± 8.2
	4.75–5.00	4.87	0.425	26.6 ± 3.4 ± 4.5
	5.00–5.50	5.21	0.454	10.8 ± 1.4 ± 1.8
	5.50–6.00	5.71	0.498	6.8 ± 1.1 ± 1.1
	6.00–7.00	6.36	0.554	1.77 ± 0.39 ± 0.33
0.15–0.25	4.00–4.25	4.12	0.359	89.7 ± 7.6 ± 20.6
	4.25–4.50	4.37	0.381	64.2 ± 6.2 ± 11.7
	4.50–4.75	4.62	0.403	44.7 ± 4.6 ± 7.8
	4.75–5.00	4.87	0.425	20.3 ± 3.2 ± 3.6
	5.00–5.50	5.21	0.454	15.0 ± 1.8 ± 2.5
	5.50–6.00	5.71	0.498	5.4 ± 1.1 ± 0.9
	6.00–7.00	6.36	0.554	1.63 ± 0.39 ± 0.31
0.25–0.35	4.00–4.25	4.12	0.359	84.1 ± 7.8 ± 18.4
	4.25–4.50	4.37	0.381	52.8 ± 6.0 ± 10.0
	4.50–4.75	4.62	0.403	30.7 ± 4.4 ± 5.8
	4.75–5.00	4.87	0.425	17.8 ± 3.0 ± 3.1
	5.00–5.50	5.21	0.454	11.4 ± 1.7 ± 1.9
	5.50–6.00	5.71	0.498	3.2 ± 0.9 ± 0.6
	6.00–7.00	6.36	0.554	1.09 ± 0.35 ± 0.36
0.35–0.45	4.00–4.25	4.12	0.359	53.7 ± 7.8 ± 18.2
	4.25–4.50	4.37	0.381	29.2 ± 5.3 ± 8.9
	4.50–4.75	4.62	0.403	19.2 ± 4.5 ± 6.0
	4.75–5.00	4.87	0.425	14.9 ± 3.2 ± 3.7
	5.00–5.50	5.21	0.454	4.9 ± 1.4 ± 1.4
	5.50–6.00	5.71	0.498	4.1 ± 1.1 ± 0.9
	6.00–7.00	6.36	0.554	0.25 ± 0.20 ± 0.25
0.45–0.55	4.00–4.25	4.12	0.359	67.3 ± 12.9 ± 28.2
	4.25–4.50	4.37	0.381	39.1 ± 8.6 ± 19.9
	4.50–4.75	4.62	0.403	21.7 ± 5.3 ± 8.1
	4.75–5.00	4.87	0.425	8.1 ± 3.2 ± 3.2
	5.00–5.50	5.21	0.454	3.3 ± 1.5 ± 1.3
	5.50–6.00	5.71	0.498	1.1 ± 0.6 ± 0.6
	6.00–7.00	6.36	0.554	0.29 ± 0.23 ± 0.26

Table 27. The invariant cross section for single prompt photon production in π^-–proton collisions at incident beam momentum 280 GeV/c, as a function of the photon's transverse momentum, in four x_F regions from −0.45 to 0.45, as measured by the CERN WA70 experiment.

CERN WA70 Bonesini *et al* 1988	π^- p → γ X			$\sqrt{s} = 22.94$ GeV *Z. Phys.* C **37** 535
x_F	p_T (GeV/c)	$\langle p_T \rangle$ (GeV/c)	$\langle x_T \rangle$	$E\mathrm{d}^3\sigma/\mathrm{d}p^3$ (pb/GeV^2)
−0.45 – −0.15	4.00–4.25	4.12	0.359	49.657 ± 3.646 ± 10.618
	4.25–4.50	4.37	0.381	33.863 ± 2.646 ± 5.935
	4.50–4.75	4.62	0.403	21.322 ± 1.929 ± 3.605
	4.75–5.00	4.87	0.425	14.941 ± 1.563 ± 2.378
	5.00–5.50	5.21	0.454	5.386 ± 0.659 ± 0.881
	5.50–6.00	5.71	0.498	3.416 ± 0.457 ± 0.545
	6.00–7.00	6.36	0.554	0.661 ± 0.284 ± 0.123
−0.15 – 0.15	4.00–4.25	4.12	0.359	102.447 ± 4.095 ± 20.375
	4.25–4.50	4.37	0.381	71.666 ± 3.374 ± 12.486
	4.50–4.75	4.62	0.403	45.872 ± 2.456 ± 7.019
	4.75–5.00	4.87	0.425	26.642 ± 1.855 ± 4.106
	5.00–5.50	5.21	0.454	12.989 ± 0.914 ± 1.994
	5.50–6.00	5.71	0.498	6.848 ± 0.622 ± 1.075
	6.00–7.00	6.36	0.554	1.640 ± 0.420 ± 0.274
0.15 – 0.45	4.00–4.25	4.12	0.359	72.425 ± 4.056 ± 14.986
	4.25–4.50	4.37	0.381	46.377 ± 3.083 ± 8.057
	4.50–4.75	4.62	0.403	28.701 ± 2.228 ± 4.571
	4.75–5.00	4.87	0.425	16.099 ± 1.600 ± 2.561
	5.00–5.50	5.21	0.454	9.979 ± 0.876 ± 1.550
	5.50–6.00	5.71	0.498	3.935 ± 0.509 ± 0.627
	6.00–7.00	6.36	0.554	1.016 ± 0.372 ± 0.182
−0.45 – 0.45	4.00–4.25	4.12	0.359	78.989 ± 2.280 ± 15.575
	4.25–4.50	4.37	0.381	54.472 ± 1.804 ± 9.041
	4.50–4.75	4.62	0.403	34.838 ± 1.327 ± 5.232
	4.75–5.00	4.87	0.425	20.614 ± 1.001 ± 3.114
	5.00–5.50	5.21	0.454	10.235 ± 0.494 ± 1.555
	5.50–6.00	5.71	0.498	4.930 ± 0.316 ± 0.767
	6.00–7.00	6.36	0.554	1.180 ± 0.217 ± 0.195
	7.00–8.00	7.36	0.642	0.205 ± 0.092 ± 0.057

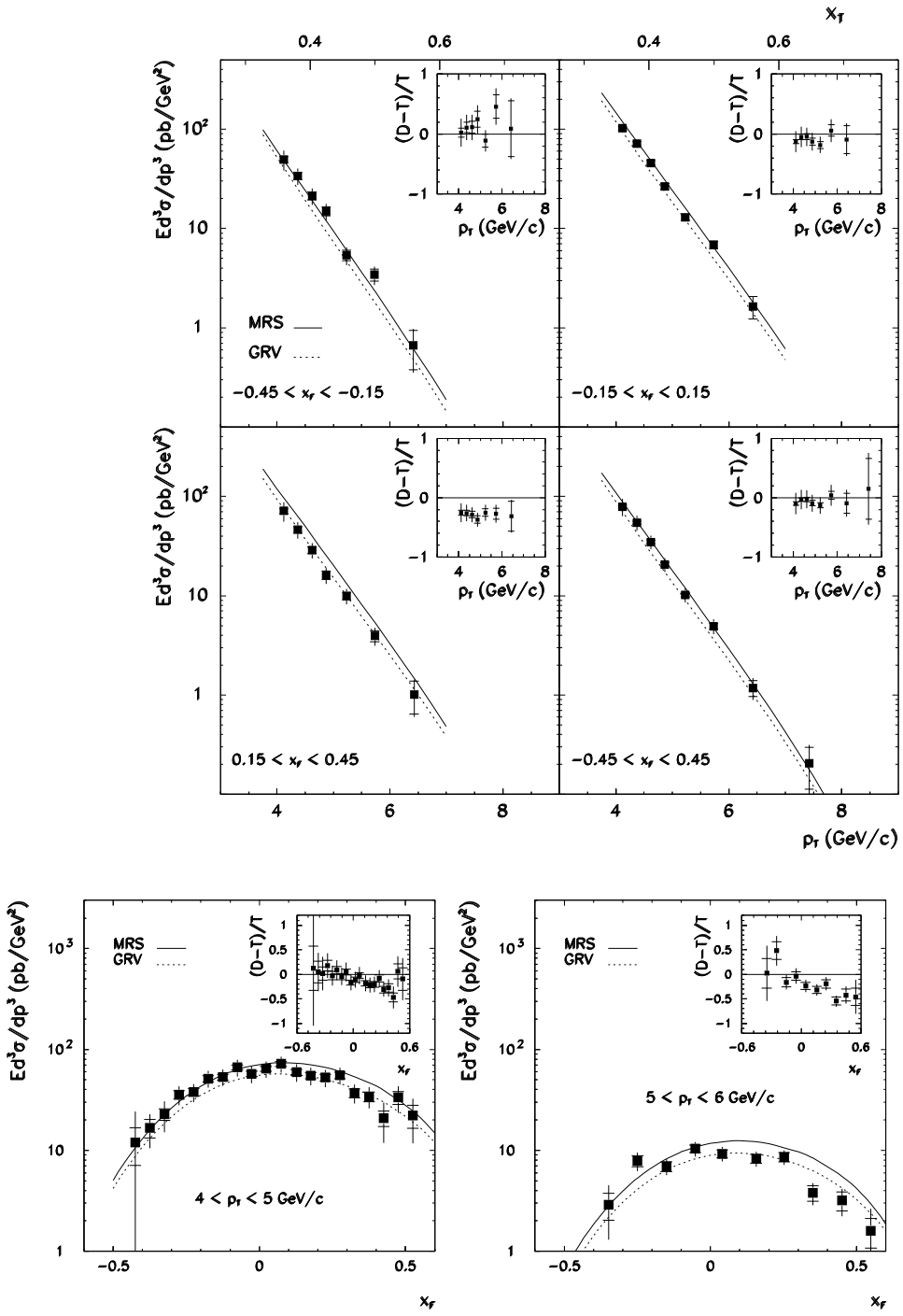

Figure 25. The WA70 π^-–proton prompt photon p_T and x_F distributions. The theoretical predictions are displayed together with the $(D-T)/T$ comparisons in the insets.

Table 28. The invariant cross section for single prompt photon production in π^-–proton collisions at incident beam momentum 280 GeV/c, as a function of x_F, in two p_T regions from 4 to 6 GeV/c, as measured by the CERN WA70 experiment.

CERN WA70 Bonesini *et al* 1988	π^- p $\rightarrow \gamma$ X	$\sqrt{s} = 22.94$ GeV *Z. Phys.* C **37** 535
p_T (GeV/c)	x_F	x_F^{mid}	$E\mathrm{d}^3\sigma/\mathrm{d}p^3$ (pb/GeV^2)
4.0–5.0	−0.45 – −0.40	−0.425	11.92 ± 4.81 ± 11.49
	−0.40 – −0.35	−0.375	16.70 ± 3.50 ± 5.16
	−0.35 – −0.30	−0.325	22.81 ± 3.07 ± 7.07
	−0.30 – −0.25	−0.275	35.58 ± 3.35 ± 6.94
	−0.25 – −0.20	−0.225	37.70 ± 3.20 ± 7.14
	−0.20 – −0.15	−0.175	51.39 ± 3.51 ± 9.09
	−0.15 – −0.10	−0.125	53.25 ± 3.45 ± 9.16
	−0.10 – −0.05	−0.075	66.33 ± 3.81 ± 11.71
	−0.05 – 0.00	−0.025	57.21 ± 3.56 ± 10.22
	0.00 – 0.05	0.025	64.29 ± 3.79 ± 11.31
	0.05 – 0.10	0.075	71.88 ± 4.01 ± 12.25
	0.10 – 0.15	0.125	59.51 ± 3.91 ± 11.24
	0.15 – 0.20	0.175	54.94 ± 3.90 ± 10.17
	0.20 – 0.25	0.225	52.55 ± 3.92 ± 9.59
	0.25 – 0.30	0.275	55.52 ± 4.20 ± 9.78
	0.30 – 0.35	0.325	37.00 ± 3.66 ± 6.87
	0.35 – 0.40	0.375	33.99 ± 3.84 ± 7.09
	0.40 – 0.45	0.425	20.82 ± 3.60 ± 8.25
	0.45 – 0.40	0.475	33.38 ± 4.85 ± 8.59
	0.50 – 0.55	0.525	22.18 ± 5.67 ± 8.78
5.0–6.0	−0.40 – −0.30	−0.35	2.89 ± 0.86 ± 1.34
	−0.30 – −0.20	−0.25	7.87 ± 0.96 ± 1.31
	−0.20 – −0.10	−0.15	6.92 ± 0.77 ± 0.98
	−0.10 – 0.00	−0.05	10.39 ± 0.93 ± 1.39
	0.00 – 0.10	0.05	9.26 ± 0.88 ± 1.24
	0.10 – 0.20	0.15	8.29 ± 0.85 ± 1.09
	0.20 – 0.30	0.25	8.58 ± 0.90 ± 1.10
	0.30 – 0.40	0.35	3.80 ± 0.68 ± 0.64
	0.40 – 0.50	0.45	3.19 ± 0.67 ± 0.70
	0.50 – 0.60	0.55	1.60 ± 0.52 ± 0.89

Table 29. The invariant cross section for single prompt photon production in π^-–proton collisions at incident beam momentum 300 GeV/c, as a function of the photon's transverse momentum, in the region $-0.65 < y < 0.52$, as measured by the CERN NA24 experiment. There is an additional 7% uncertainty in the normalization.

CERN NA24	π^- p $\to \gamma$ X	$\sqrt{s} = 23.75$ GeV
De Marzo *et al* 1987		*Phys. Rev.* D **36** 8

y	p_T (GeV/c)	$p_T^{\rm mid}$ (GeV/c)	$x_T^{\rm mid}$	$E{\rm d}^3\sigma/{\rm d}p^3$ (pb/GeV^2)
−0.65–0.52	2.5–3.0	2.75	0.232	3030.0 ± 490.0 ± 700.0
	3.0–3.5	3.25	0.274	778.0 ± 69.0 ± 170.0
	3.5–4.0	3.75	0.316	294.0 ± 34.0 ± 36.0
	4.0–4.5	4.25	0.358	89.3 ± 3.4 ± 8.8
	4.5–5.5	5.00	0.421	21.0 ± 1.1 ± 2.2
	5.5–6.5	6.00	0.505	2.55 ± 0.34 ± 0.13
	6.5–7.5	7.00	0.589	0.369 ± 0.140 ± 0.012

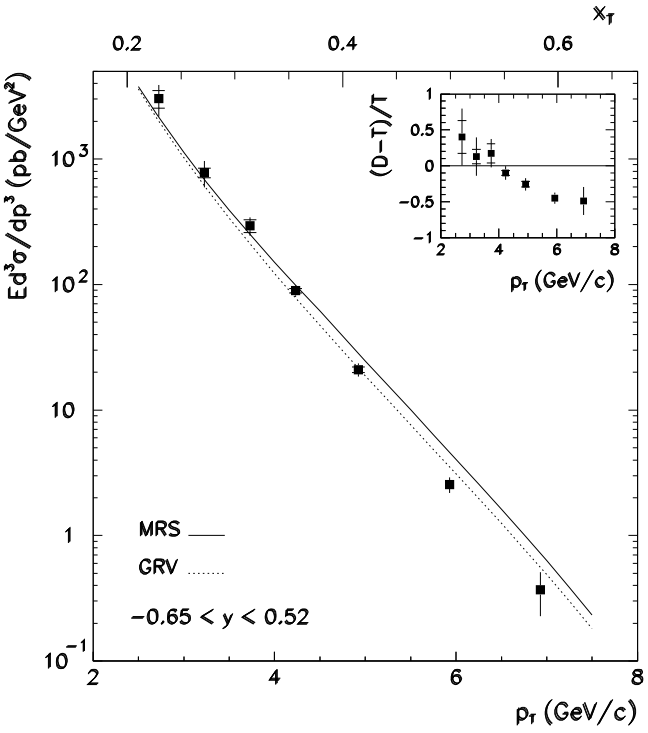

Figure 26. The NA24 π^-–proton prompt photon p_T distribution. The theoretical predictions are displayed together with the $(D-T)/T$ comparison in the inset.

Table 30. The invariant cross section for single prompt photon production in π^+–carbon collisions at incident beam momentum 200 GeV/c, as a function of the photon's transverse momentum, in the region $-0.75 < y < 0.2$, as measured by the Fermilab E629 experiment. The errors include systematic uncertainties.

FNAL E629	π^+ C $\rightarrow \gamma$ X	$\sqrt{s} = 19.40$ GeV
McLaughlin *et al* 1983		*Phys. Rev. Lett.* **51** 971

y	p_T (GeV/c)	$p_T^{\rm mid}$ (GeV/c)	$x_T^{\rm mid}$	$E{\rm d}^3\sigma/{\rm d}p^3$ (pb/GeV^2)
−0.75–0.20	2.1–2.3	2.20	0.227	<25000
	2.3–2.6	2.45	0.253	< 6400
	2.6–3.0	2.80	0.289	1200 ± 2200
	3.0–3.5	3.25	0.335	1000 ± 700
	3.5–4.0	3.75	0.387	430 ± 290
	4.0–5.0	4.50	0.464	78 ± 67
	5.0–6.0	5.50	0.567	33 ± 37

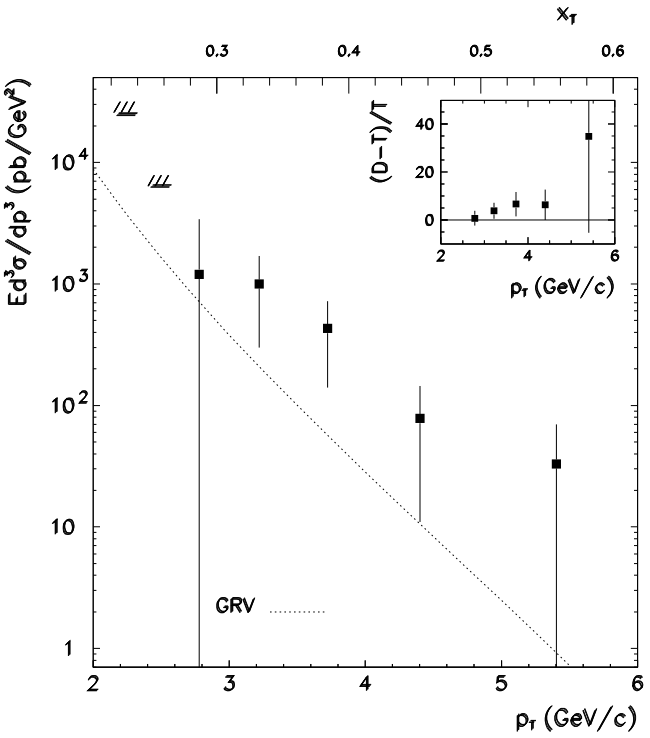

Figure 27. The E629 π^+–carbon prompt photon p_T distribution. The theoretical prediction using the GRV94 structure function parametrisation is shown together with the $(D-T)/T$ comparison in the inset. The kinematical range in p_T is too low for the applicability of MRS or CTEQ sets.

Table 31. The invariant cross section for single prompt photon production in π^+–carbon collisions at incident beam momentum 200 GeV/c, as a function of the photon's transverse momentum, in the region $-0.4 < y < 1.2$, as measured by the CERN NA3 experiment. Data are given for two different experimental conditions described as (a) the conversion trigger and (b) the calorimeter trigger. Additional systematic errors are ≈30% for (a) and ≈40% for (b)

CERN NA3	π^+ C $\rightarrow \gamma$ X	$\sqrt{s} = 19.40$ GeV
Badier *et al* 1986		*Z. Phys.* C **31** 341

	y	$\langle p_T \rangle$ (GeV/c)	$\langle x_T \rangle$	$E\mathrm{d}^3\sigma/\mathrm{d}p^3$ (pb/GeV^2)
(a)				
	−0.4–1.2	2.94	0.303	23000 ± 5730
		3.09	0.319	16000 ± 2520
		3.33	0.343	7390 ± 1090
		3.70	0.381	2400 ± 390
		4.21	0.434	330 ± 130
		4.98	0.513	38 ± 18
(b)				
	−0.4–0.8	3.90	0.402	1000 ± 300
		4.10	0.423	880 ± 190
		4.30	0.443	420 ± 120
		4.50	0.464	250 ± 80
		4.70	0.485	83 ± 55
		5.00	0.515	100 ± 25

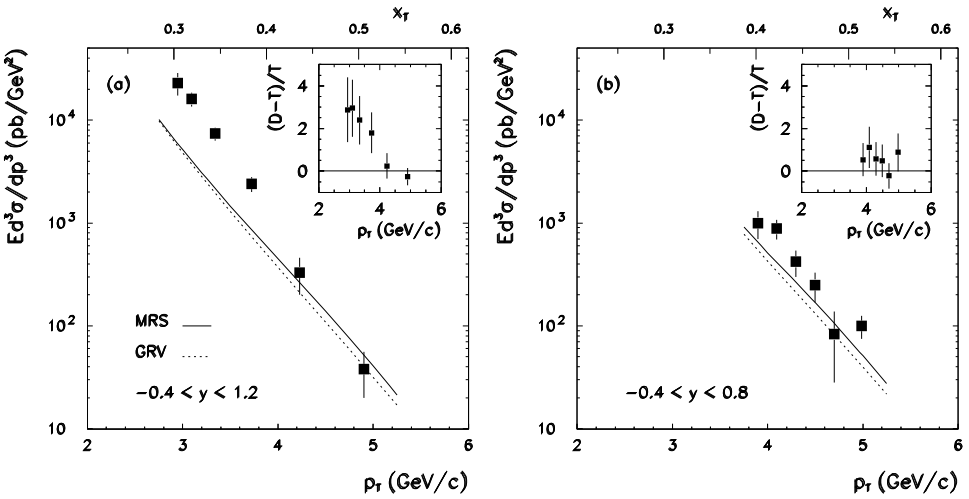

Figure 28. The NA3 π^+–carbon prompt photon p_T distributions. The theoretical predictions are displayed together with the $(D - T)/T$ comparisons in the insets.

Table 32. The invariant cross section for single prompt photon production in π^-–carbon collisions at incident beam momentum 200 GeV/c, as a function of the photon's transverse momentum, in the region $-0.4 < y < 1.2$, as measured by the CERN NA3 experiment. Data are given for two different experimental conditions described as (a) the conversion trigger and (b) the calorimeter trigger. Additional systematic errors are ≈30% for (a) and ≈40% for (b)

CERN NA3	π^- C $\rightarrow \gamma$ X	$\sqrt{s} = 19.40$ GeV
Badier *et al* 1986		*Z. Phys.* C **31** 341

y	$\langle p_T \rangle$ (GeV/c)	$\langle x_T \rangle$	$E\mathrm{d}^3\sigma/\mathrm{d}p^3$ (pb/GeV^2)
(a)			
−0.4–1.2	2.94	0.303	25300 ± 4700
	3.09	0.319	14400 ± 1930
	3.33	0.343	8170 ± 850
	3.70	0.381	2130 ± 280
	4.21	0.434	710 ± 110
	4.98	0.513	85 ± 17
(b)			
−0.4–0.8	3.90	0.402	1300 ± 300
	4.10	0.423	1400 ± 200
	4.30	0.443	670 ± 130
	4.50	0.464	320 ± 90
	4.70	0.485	280 ± 60
	5.00	0.515	110 ± 30

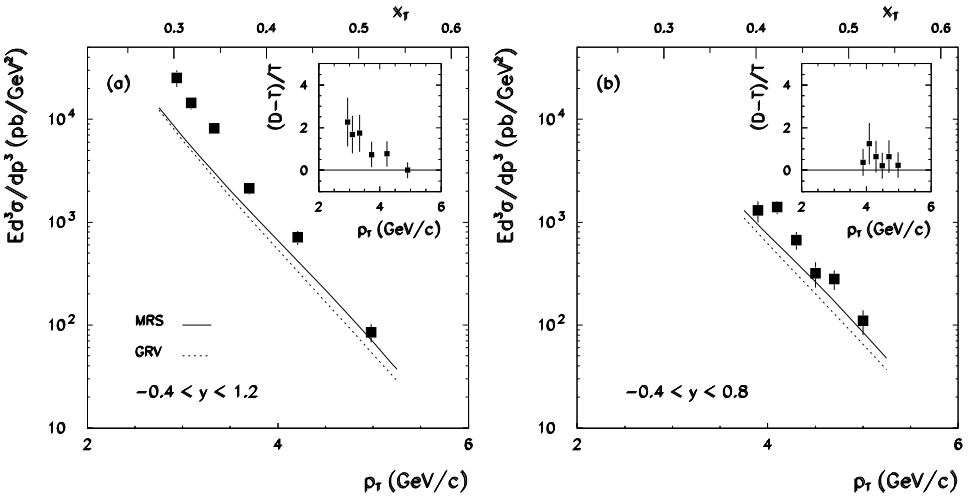

Figure 29. The NA3 π^-–carbon prompt photon p_T distributions. The theoretical predictions are displayed together with the $(D-T)/T$ comparisons in the insets.

Table 33. The invariant cross section for single prompt photon production in π^-–beryllium collisions at incident beam momentum 500 GeV/c, as a function of the photon's transverse momentum, in four y ranges from -0.7 to 0.7, as measured by the Fermilab E706 experiment.

FNAL E706	π^- Be $\rightarrow \gamma$ X	$\sqrt{s} = 30.63$ GeV
Alverson *et al* 1993		*Phys. Rev.* D **48** 5

y	p_T (GeV/c)	$p_T^{\rm mid}$ (GeV/c)	$x_T^{\rm mid}$	$E{\rm d}^3\sigma/{\rm d}p^3$ (pb/GeV^2)
-0.7 – -0.2	4.0 – 4.5	4.25	0.278	215.0 ± 43.0 ± 53.0
	4.5 – 5.0	4.75	0.310	83.0 ± 16.0 ± 17.0
	5.0 – 5.5	5.25	0.343	29.0 ± 8.0 ± 6.0
	5.5 – 6.0	5.75	0.375	12.0 ± 4.0 ± 2.0
	6.0 – 7.0	6.50	0.424	4.2 ± 1.3 ± 0.8
	7.0 –10.0	8.50	0.555	0.38 ± 0.18 ± 0.07
-0.2 – 0.2	3.5 – 4.0	3.75	0.245	690.0 ± 150.0 ± 160.0
	4.0 – 4.5	4.25	0.278	252.0 ± 45.0 ± 51.0
	4.5 – 5.0	4.75	0.310	126.0 ± 18.0 ± 23.0
	5.0 – 5.5	5.25	0.343	46.0 ± 9.0 ± 8.0
	5.5 – 6.0	5.75	0.375	22.0 ± 6.0 ± 4.0
	6.0 – 7.0	6.50	0.424	5.9 ± 1.7 ± 1.0
	7.0 – 10.0	8.50	0.555	0.23 ± 0.16 ± 0.04
0.2 – 0.7	3.5 – 4.0	3.75	0.245	647.0 ± 130.0 ± 190.0
	4.0 – 4.5	4.25	0.278	117.0 ± 35.0 ± 39.0
	4.5 – 5.0	4.75	0.310	83.0 ± 15.0 ± 19.0
	5.0 – 5.5	5.25	0.343	30.0 ± 8.0 ± 6.0
	5.5 – 6.0	5.75	0.375	13.0 ± 4.0 ± 3.0
	6.0 – 7.0	6.50	0.424	6.5 ± 1.5 ± 1.2
	7.0 – 10.0	8.50	0.555	0.18 ± 0.15 ± 0.03
-0.7 – 0.7	3.5 – 3.75	3.625	0.237	654.0 ± 140.0 ± 210.0
	3.75 – 4.0	3.825	0.250	355.0 ± 88.0 ± 98.0
	4.0 – 4.25	4.125	0.269	280.0 ± 39.0 ± 63.0
	4.25 – 4.5	4.325	0.282	101.0 ± 25.0 ± 25.0
	4.5 – 4.75	4.625	0.302	131.0 ± 16.0 ± 26.0
	4.75 – 5.0	4.825	0.318	58.0 ± 10.0 ± 11.0
	5.0 – 5.5	5.25	0.343	34.0 ± 5.0 ± 6.0
	5.5 – 6.0	5.75	0.375	15.0 ± 3.0 ± 3.0
	6.0 – 7.0	6.50	0.424	5.5 ± 0.9 ± 1.0
	7.0 – 8.0	7.50	0.490	0.46 ± 0.24 ± 0.08
	8.0 – 10.0	9.0	0.588	0.16 ± 0.08 ± 0.03

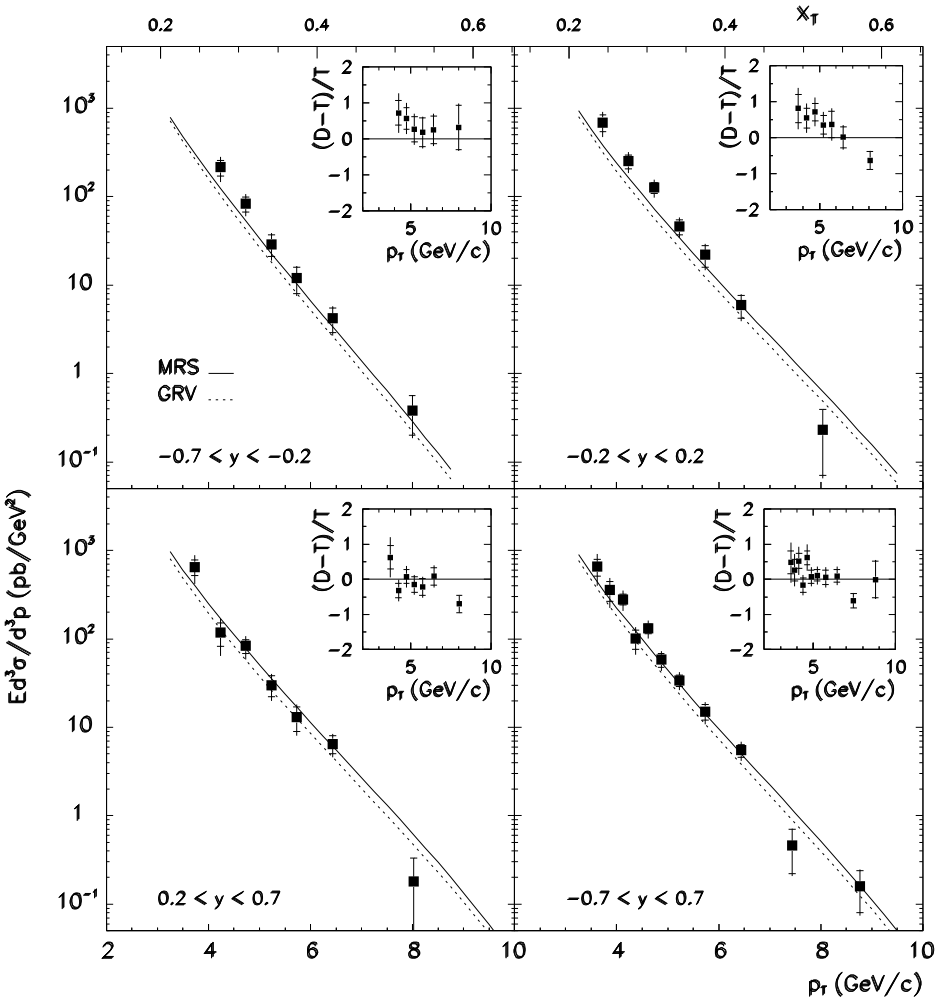

Figure 30. The E706 π^-–beryllium prompt photon p_T distributions. The theoretical predictions are displayed together with the $(D-T)/T$ comparisons in the insets.

Combined data comparison plot for p p → γ X

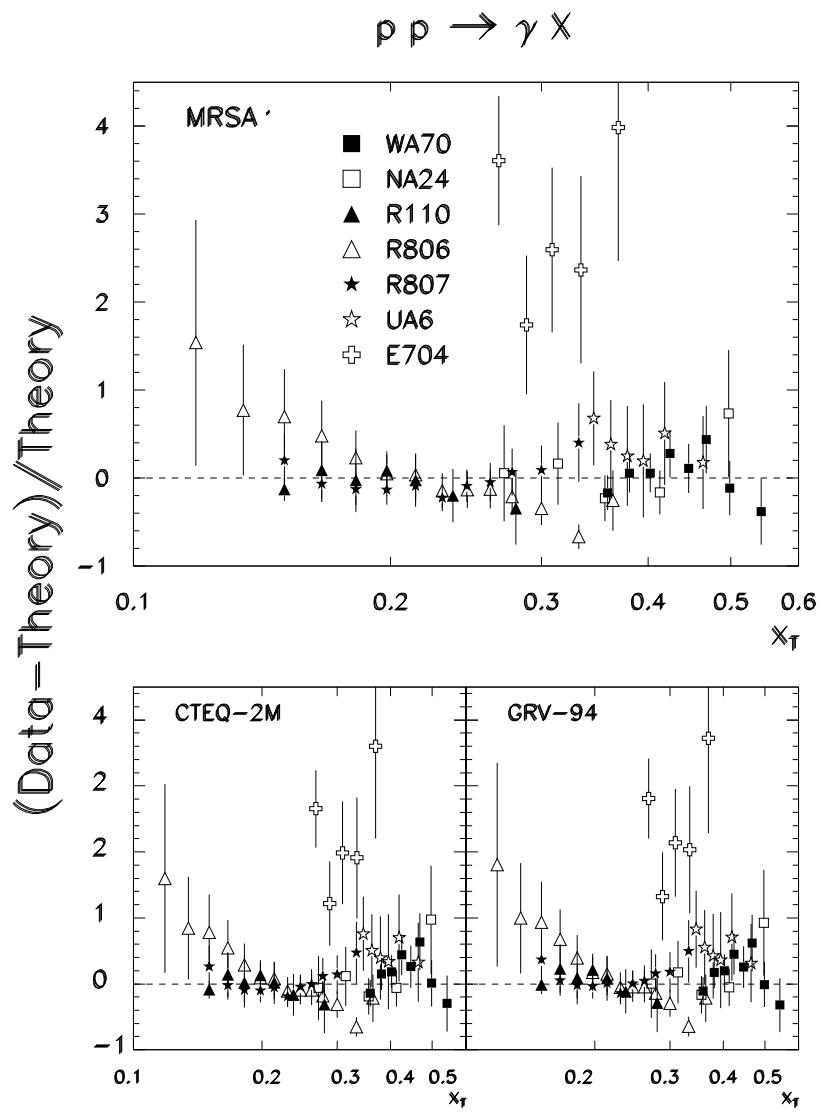

Figure 31. Compilation of data on the relative differences between the measured pp → γX cross sections and the theoretical predictions, described in the text, for the different structure function parametrisations.

Combined data comparison plot for $\bar{p}\,p \to \gamma\,X$

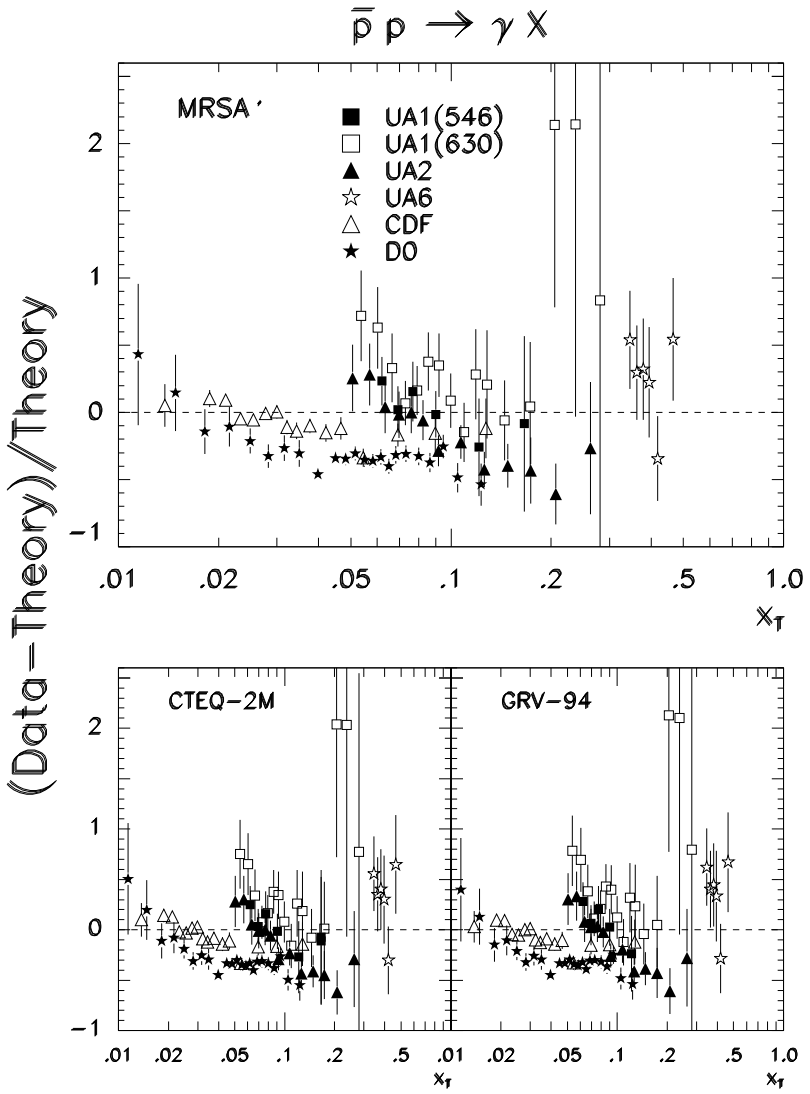

Figure 32. Compilation of data on the relative differences between the measured $\bar{p}\,p \to \gamma\,X$ cross sections and the theoretical predictions, described in the text, for the different structure function parametrisations.

Combined data comparison plot for p nucleus → γ X

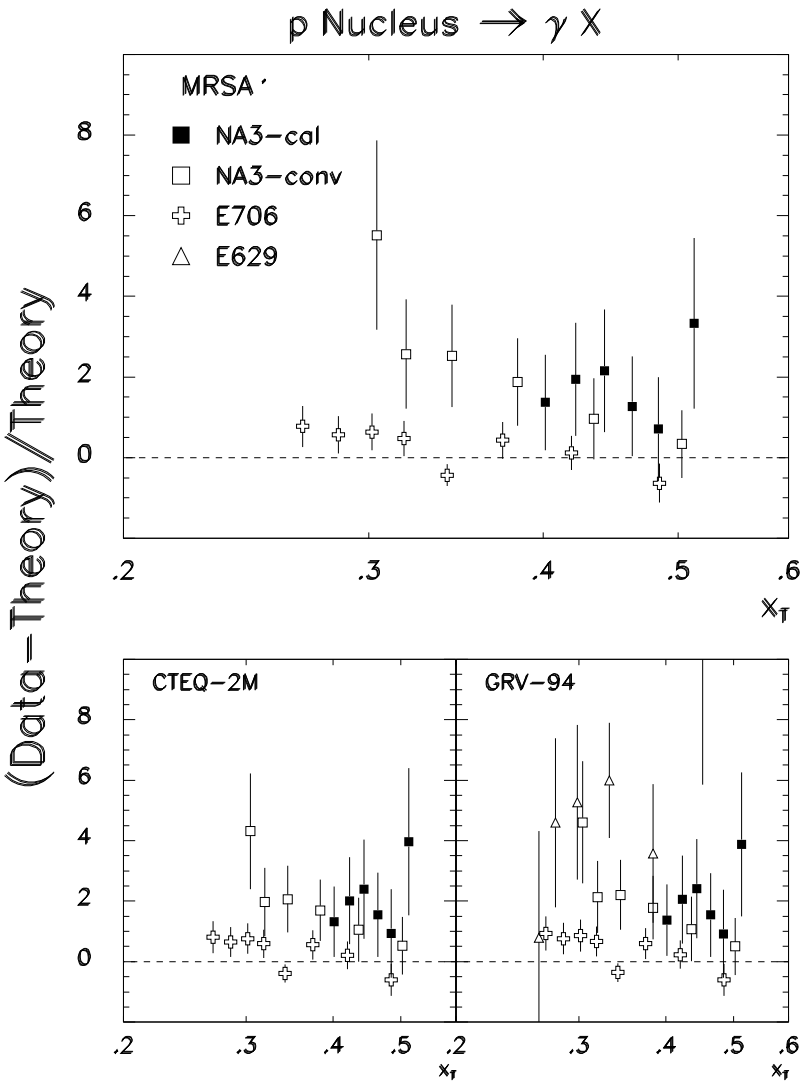

Figure 33. Compilation of data on the relative differences between the measured p nucleus → γ X cross sections and the theoretical predictions, described in the text, for the different structure function parametrisations.

Combined data comparison plots for $\pi^{\pm}$ p $\rightarrow \gamma$ X and $\pi^{\pm}$ nucleus $\rightarrow \gamma$ X

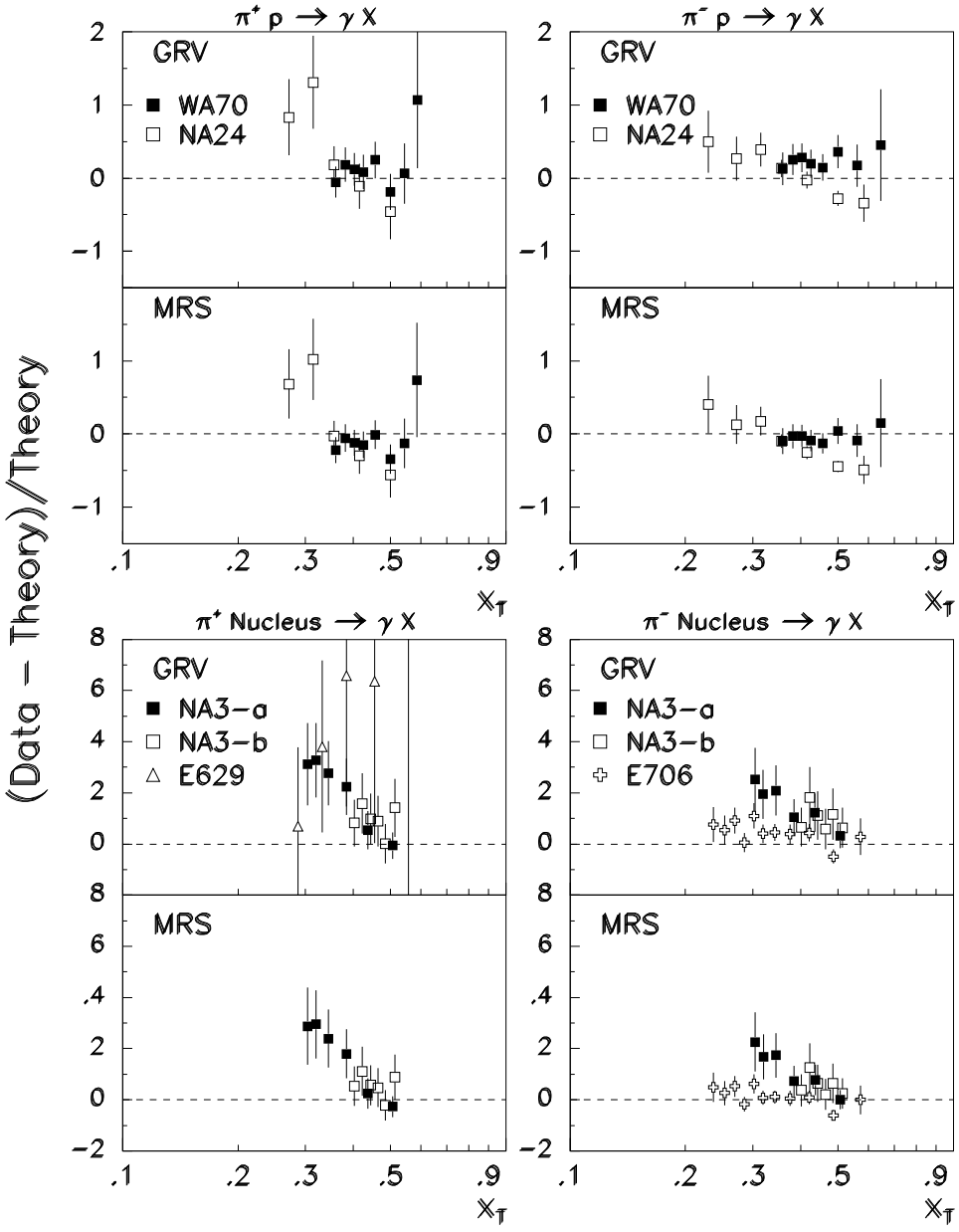

Figure 34. Compilation of data on the relative differences between the measured π p $\rightarrow \gamma$ X and π nucleus $\rightarrow \gamma$ X cross sections and the theoretical predictions, as described in the text, for the different structure function parametrisations.

3. The two-photon data

Table 34. Data on prompt two-photon production

Collaboration	$\sqrt{s}$	Beam	Target	Measurement
R806 [16]	63	p	p	$\mathrm{d}^2\sigma/\mathrm{d}y\mathrm{d}m_{\gamma\gamma}$
R807 [19]	63	p	p	$\mathrm{d}^2\sigma/\mathrm{d}y\mathrm{d}m_{\gamma\gamma}$
UA2 [20]	630	$\bar{\mathrm{p}}$	p	$\mathrm{d}\sigma/\mathrm{d}p_T$
UA2 [21]	630	$\bar{\mathrm{p}}$	p	$\mathrm{d}^2\sigma/\mathrm{d}\eta_1/\mathrm{d}\eta_2$
UA1 [22]	630	$\bar{\mathrm{p}}$	p	σ $E\mathrm{d}^3\sigma/\mathrm{d}p^3$
E741(CDF) [24]	1800	$\bar{\mathrm{p}}$	p	σ $\mathrm{d}\sigma/\mathrm{d}p_T$
NA24 [6]	23.7	π^-	p	$E\mathrm{d}^3\sigma/\mathrm{d}p^3$
WA70 [9]	22.96	π^-	p	σ $\mathrm{d}\sigma/\mathrm{d}p_T$
NA3 [4]	19.4	p	C	σ

Table 35. Differential cross section for the production of two direct photons in proton–proton interactions at a centre-of-mass energy of 63 GeV as measured by the CERN ISR R806 experiment. A single data point is reported at $y_{cm} = 0$ and in the two-photon mass range 8 to 11 GeV/c^2.

CERN R806 Kourkoumelis *et al* 1982	$pp \to \gamma\gamma$ X	$\sqrt{s} = 63$ GeV *Z. Phys.* C **16** 101
y_{cm}	$p_T^{\gamma_1,\gamma_2}$ (GeV/c)	$m_{\gamma\gamma}$ (GeV/c^2)	$d^2\sigma/dy dm_{\gamma\gamma}$ (pb/GeV)
0.0	>3	8–11	80 ± 40

Table 36. Differential cross section for the production of two direct photons in proton–proton interactions at a centre-of-mass energy of 63 GeV as measured by the CERN ISR R807 (AFS) experiment. Data are reported in the central rapidity region for two two-photon mass ranges for events with both photons having transverse momentum greater than 2 GeV/c.

CERN R807 Åkesson *et al* 1986	p p $\to \gamma\gamma$ X	$\sqrt{s} = 63$ GeV *Z. Phys.* C **32** 491
$\lvert y_{cm}\rvert$	$p_T^{\gamma_1,\gamma_2}$ (GeV/c)	$m_{\gamma\gamma}$ (GeV/c^2)	$d^2\sigma/dy dm_{\gamma\gamma}$ (pb/GeV)
<0.5	>2	2.2–4.0	8300 ± 6100
		4.0–6.0	550 ± 270

Table 37. The differential cross section, as a function of the transverse momentum of one photon, for two isolated prompt photons produced in proton–antiproton collisions at a centre-of-mass energy of 630 GeV, as measured by the CERN UA2 experiment. The errors shown are statistical plus p_T dependent systematic errors. There is an additional 6.8% overal systematic error.

CERN UA2 Alitti *et al* 1992	$\bar{\mathrm{p}}\,\mathrm{p} \to \gamma\gamma\ \mathrm{X}$		$\sqrt{s} = 630$ GeV *Phys. Lett.* **288B** 386
$\lvert\eta^{\gamma_1,\gamma_2}\rvert$	$p_T^{\gamma_1,\gamma_2}$ (GeV/c)	$\langle p_T^{\gamma_1,\gamma_2}\rangle$ (GeV/c)	$\mathrm{d}\sigma/\mathrm{d}p_T$ (pb/GeV)
<0.76	10–12	10.9	4.31 ± 1.03
	12–18	14.1	0.922 ± 0.33
	18–24	20.4	0.346 ± 0.125
	24–31	26.9	0.116 ± 0.063

Table 38. The double differential cross section, as a function of pseudorapidity, for two isolated prompt photons produced in proton–antiproton collisions at a centre-of-mass energy of 630 GeV, as measured by the CERN UA2 experiment. These data come from a sample of 4 events with both photons p_T greater than 11 GeV and |pseudorapidities| less than 0.83.

CERN UA2 Ansari *et al* 1988	$\bar{\mathrm{p}}\,\mathrm{p} \to \gamma\gamma\ \mathrm{X}$	$\sqrt{s} = 630$ GeV *Z. Phys.* **C41** 395
$\lvert\eta^{\gamma_1,\gamma_2}\rvert$	$p_T^{\gamma_1,\gamma_2}$ (GeV/c)	$\mathrm{d}\sigma/\mathrm{d}\eta_1\mathrm{d}\eta_2$ (pb)
<0.83	>11.0	4.8 ± 2.5

Table 39. Cross section for two isolated photon production in proton–antiproton collisions at a centre-of-mass energy of 630 GeV measured by the CERN UA1 experiment. Total cross sections are given for |pseudorapidity| < 3, first requiring both photons to have $E_T > 12$ GeV and second with the additional cut on z where $z = -\vec{E}_{T1} \cdot \vec{E}_{T2}/E_{T1}^2$. Finally the cross section is transformed to a value for $E\mathrm{d}^3\sigma/\mathrm{d}p^3$ at one point.

CERN UA1 Albajar *et al* 1988		$\bar{\mathrm{p}}\,\mathrm{p} \to \gamma\gamma\ \mathrm{X}$	$\sqrt{s} = 630$ GeV *Phys. Lett.* **209B** 385
$\lvert\eta\rvert$	z	$E_T^{\gamma_1,\gamma_2}$ (GeV)	σ (pb)
< 3	—	>12	$38 \pm 19 \pm 10$
$\lvert\eta\rvert$	z	$E_T^{\gamma_1}$ (GeV)	σ (pb)
< 3	$>12/E_T^{\gamma_1}$	> 12	$63 \pm 32 \pm 17$
η	z	E_T^{γ} (GeV)	$E\mathrm{d}^3\sigma/\mathrm{d}p^3$ (pb/GeV^2)
0.0	>0.6	20	$0.0057 \pm 0.0029 \pm 0.0015$

Table 40. The differential cross section, as a function of the transverse momentum of each photon, for two isolated prompt photons produced in proton–antiproton collisions at a centre-of-mass energy of 1800 GeV, as measured by the Fermilab E741 (CDF) experiment.

FNAL E741(CDF) Abe *et al* 1993		$\bar{\mathrm{p}}\,\mathrm{p} \to \gamma\gamma\ \mathrm{X}$	$\sqrt{s} = 1800$ GeV *Phys. Rev. Lett.* **70** 2232
$\lvert\eta\rvert$	p_T (GeV/c)	$\langle p_T \rangle$ (GeV/c)	$\mathrm{d}\sigma/\mathrm{d}p_T$ (pb/GeV)
<0.9	10–12	11.1	$17.5 \pm 10.0^{+5.4}_{-3.7}$
	12–15	13.5	$11.6 \pm 5.3^{+2.3}_{-4.1}$
	15–19	17.4	$4.2 \pm 2.7^{+1.7}_{-1.2}$
	10–19	13.3	$9.6 \pm 3.0^{+3.6}_{-2.6}$
			σ (pb)
<0.9	10–19		$86 \pm 27^{+32}_{-23}$

Table 41. The invariant cross section for inclusive two-photon production, versus the transverse momentum of one of the photons, in π^-–proton collisions at an incident beam momentum of 300 GeV/c as measured by the CERN NA24 experiment. The cross section is integrated over $z = \vec{p}^{\,\gamma}_{T1} \cdot \vec{p}^{\,\gamma}_{T2}/(\vec{p}^{\,\gamma}_{T1})^2$ of the other photon above a value $z^{\min} = p^{\min}_{T2}/p^{\min}_{T1}$, where $p^{\min}_{T1}$ is the lower edge of the considered bin of the transverse momentum p^{γ}_{T1} and $p^{\min}_{T2}$ is 2 GeV/c.

CERN NA24 π^- p $\rightarrow \gamma\gamma$ X $\sqrt{s} = 23.7$ GeV
De Marzo *et al* 1990 *Phys. Rev.* **D42** 748

p_{T1} (GeV/c)	$p^{\rm mid}_{T1}$ (GeV/c)	$z^{\min}$	$E{\rm d}^3\sigma/{\rm d}p^3$ (pb/GeV^2)
2.5–3.0	2.75	0.80	$2.07\ ^{+0.53}_{-0.92}$
3.0–4.0	3.50	0.67	$0.70\ ^{+0.23}_{-0.36}$
4.0–5.0	4.50	0.50	$0.093\ ^{+0.133}_{-0.093}$

Table 42. Cross sections, as a function of the transverse momentum of one of the photons, for direct two-photons produced in π^-–proton collisions at incident beam momentum 280 GeV/c, as measured by the CERN WA70 experiment. The first section gives the cross section for two-photon production integrated over the allowed rapidity range and over the two given transverse momenta. The second two sections have the the requirement that $z = \vec{p}^{\,\gamma}_{T1} \cdot \vec{p}^{\,\gamma}_{T2}/(\vec{p}^{\,\gamma}_{T1})^2$ be greater than $z_{\rm min} = 2.75/p_{T1}$.

CERN WA70 π^- p $\rightarrow \gamma\gamma$ X $\sqrt{s} = 22.96$ GeV
Bonvin *et al* 1989 *Z. Phys.* **C41** 591

y	p_{T1} (GeV/c)	p_{T2} (GeV/c)	σ (pb)
−1.0–1.25	>3.0	>2.75	54 ± 9

y	p_T (GeV/c)	$z_{\rm min}$	${\rm d}\sigma/{\rm d}p_T$ (pb/GeV)
−1.0–1.25	3.0–3.5	2.75/3.0	70.0 ± 17.2
	3.5–4.0	2.75/3.5	25.0 ± 8.6
	4.0–4.5	2.75/4.0	17.0 ± 5.2
	4.5–5.0	2.75/4.5	10.0 ± 3.4
	5.0–6.0	2.75/5.0	4.7 ± 1.4
	6.0–7.0	2.75/5.5	1.0 ± 0.6

y	p_T (GeV/c)	$z_{\rm min}$	σ (pb)
−1.0–1.25	>3.0	2.75/3.0	69 ± 11.5

Table 43. The direct two-photon cross section, as a function of the transverse momentum of one photon, produced in proton carbon interactions at incident beam momentum of 200 GeV/c as measured by the CERN NA3 experiment.

CERN NA3 — p C $\to \gamma\gamma$ X, π^+ C $\to \gamma\gamma$ X, π^- C $\to \gamma\gamma$ X — $\sqrt{s} = 19.4$ GeV

Badier *et al* 1985 — *Phys. Lett.* **164B** 184

	y	p_T (GeV/c)	σ (pb)
p C $\to \gamma\gamma$ X	−0.4–1.0	> 1.8	1480 ± 380
		1.8–2.0	740 ± 250
		2.0–2.5	570 ± 230
		>2.5	170 ± 130
π^+ C $\to \gamma\gamma$ X	−0.4–1.0	> 1.8	350 ± 640
π^- C $\to \gamma\gamma$ X	−0.4–1.0	> 1.8	1220 ± 350
		1.8–2.0	610 ± 250
		2.0–2.5	430 ± 240
		>2.5	180 ± 140

4. How to access the Durham–RAL HEP Databases

All the data presented in this review can by retrieved from the Durham–RAL HEP Databases (HEPDATA). These databases are available on two different computing platforms.

- The World-Wide-Web (WWW) information system
- Internet service (on a UNIX machine) via TELNET

This sections briefly explains how to use these databases to retrieve selected data sets.

4.1. Using the database on the World-Wide-Web system

The HEPDATA databases are available on the World-Wide-Web (WWW) information system which is now frequently used by many physicists. If the option for HEPDATA is on your 'homepage' or if you have access to the CERN HEP page, then simply select the relevant option and form your search in a similar way to that which will described in the following section. Of course the details of listing records is different but comprehensive on-line HELP is included in the system.

If the options for HEPDATA are not available then either issue the command:

```
www http://durpdg.dur.ac.uk/HEPDATA
or
www http://129.234.8.100/HEPDATA
```

and follow through the menus to the REACTION database. If you intend to make extensive use of the HEPDATA system then ask your system administrator to include a pointer to HEPDATA in your 'homepage' using the above http address.

A user guide [54] is available. Contact m.r.whalley@durham.ac.uk for more information on the HEPDATA databases.

4.2. Using the database via TELNET on durpdg

The internet service is available over `TELNET` (`INTERNET`). It may be used directly from any machine having access to this network.

```
TELNET 129.234.8.100
or
TELNET durpdg.dur.ac.uk
```

using the guest id,

`pdg` (password `hepdata`).

You are then presented with a menu of options. You can select by number or name.

To download records to your host machine, use the `PRINT` command, and answer the questions.

This example demonstrates getting the CDF single photon data.

Comments are in italics (*like this*) and entries by the user are shown underlined (`like this`).

```
>        ************************************************
>        * THE DURHAM-RUTHERFORD HEP DATA ARCHIVE. HEPDATA *
>        ************************************************
>
>  You may select one of the following by number, or name, as you wish:
>
>  ---> 0  README          Please read this for news etc....
>  ---> 1  Help            Type 1 or Help to get HELP.
>  ---> 2  Data            Numerical values - X sects.,polarisations
>  ---> 3  Quit            Type Quit to exit from the programme.
>  ---> 4  (not used)
>  ---> 5  Particle Prop   RPP Full Listings(PDG-Berkeley).
>  ---> 6  Experiments     Information about current HEP experiments.
>  ---> 7  Slacppf         The SLAC preprint/publication/citation database
>  ---> 8  IDs (E-mail)    E-mail ids of HEP Physicists (worldwide)
>  ---> 9  Change the erase character (  )
>
> Please make your choice now:
> 2                              select option 2
>
> ......REACTION DATA Database......
> ......( last update Aug 18 ).....
>
> REACTION_DATA:Enter Command>
> find r prl 73 2662       locate the data by reference
>
> Result 1 Record(s)
>
> REACTION_DATA:Enter Command>
> list                     asks for the whole record to be listed
>
>-----------------Record 1--------------------------------------------------
> <REC-ID>   8413
> <first AUTHor>   ABE 94
> <Reference>      PRL 73, 2662
> <Date>           1994
>                  FERMILAB-PUB-94-208-E
> <Date>           JUL 1994
> <Dur.Ref.>       4264
> <SLAC-IRN>       2981688
```

```
>  Comment         Fermilab.  Measurement of the prompt photon cross
>                  section in (pbar p) collisions at centre of mass
>                  energy 1800 GeV. Data represent 6 times the
>                  luminosity of that previously published (PR D48
>                  (1993)  2998) and extend the PT range up to 115 GeV.
> <DEtector>       CDF
> <EXPeriment no.> FNAL-741
>
>                        *****DATA TABLES*****
>  TABLE-KEYS
> <REaction>       PBAR P --> GAMMA X
> <OBServable>     D2SIG/DPT/DETARAP
> <PLAB range Gev> 1.7271E+06,1.7271E+06
>  Table,Fig,Page  T 1,F 4
>  Comment         Note that the systematic uncertainties are approximately
>                  100 pct correlated bin to bin.
>
>
>      RE                      PBAR P --> GAMMA X
>      SQRT(S) IN GEV          1800
>
>          PT IN GEV           D2(SIG)/DPT/DETARAP IN PB/GEV
>
>         12.3                   4460.    +- 415.  (DSYS=714)
>         17.0                   1300.    +-  38.  (DSYS=156)
>         19.0                    805.    +-  21.  (DSYS= 89)
>         21.0                    458.    +-  15.  (DSYS= 46)
>         23.0                    308.    +-  12.  (DSYS= 31)
>
>
>(etc... lists rest of the record)
>
>
> REACTION_DATA:Enter Command>
> qq                        leaves the database
>
```

A user guide to the Internet database service [55] is available from m.r.whalley@durham.ac.uk.

5. Other Reviews in this series

Other Data Reviews in this series, and in earlier Rutherford Appleton Laboratory preprints, are listed below. Copies may be obtained by contacting one of the authors or the publishers.

A Compilation of Nucleon–Nucleon and Nucleon–Antinucleon Elastic Scattering Data M K Carter, P D B Collins and M R Whalley 1986 RAL-86-002

A Compilation of Data on the Energy–Energy Correlation and its Asymmetry in e^+e^- Annihilation W J Stirling and M R Whalley 1987 RAL-87-107

A Compilation of Data on Single Prompt Photon Production in Hadron–Hadron Interactions P Aurenche and M R Whalley 1989 RAL-89-106

A Compilation of Structure Functions in Deep Inelastic Scattering R G Roberts and M R Whalley 1991 *J. Phys G: Nucl. Part. Phys.* **17** D1–D151

A Compilation of Drell–Yan Cross Sections W J Stirling and M R Whalley 1993 *J. Phys G: Nucl. Part. Phys.* **19** D1–D102

A Compilation of Data on Two-Photon Reactions leading to Hadron Final States D Morgan, M R Pennington and M R Whalley 1994 *J. Phys G: Nucl. Part. Phys.* **20** Supplement 8A A1–A147

A Compilation of Inclusive Particle Production Data in e^+e^- Annihilation G D Lafferty, P I Reeves and M R Whalley 1995 *J. Phys G: Nucl. Part. Phys.* **21** Supplement 12A A1–A151

Acknowledgments

This research is supported by PPARC grant GR/J58817. The authors wish to thank Miss Rachel Lumpkin and Miss Lisa Flynn for their help in preparing the manuscript, and the members of the HEPDATA management committee for their guidance.
WV is grateful to L E Gordon and A Vogt for helpful discussions.

References

[1] Expt E95, Baltrusaitis R M *et al* 1979 *Phys. Lett.* **88B** 372
[2] Expt E629, McLaughlin M *et al* 1983 *Phys. Rev. Lett.* **51** 971
[3] Expt NA3, Badier J *et al* 1986 *Z. Phys.* C **31** 341
[4] Expt NA3, Badier J *et al* 1985 *Phys. Lett.* **164B** 184
[5] Expt NA24, De Marzo C *et al* 1987 *Phys. Rev.* D **36** 8
[6] Expt NA24, De Marzo C *et al* 1990 *Phys. Rev.* D **42** 748
[7] Expt WA70, Bonesini M *et al* 1988 *Z. Phys.* C **38** 371
[8] Expt WA70, Bonesini M *et al* 1988 *Z. Phys.* C **37** 535
[9] Expt WA70, Bonvin E *et al* 1989 *Z. Phys.* C **41** 591
[10] Expt E704, Adams D *et al* 1995 *Phys. Lett.* **345B** 569
[11] Expt E706, Alverson G *et al* 1993 *Phys. Rev.* D **48** 5
Alverson G *et al* 1992 *Phys. Rev. Lett.* **68** 2584
[12] Expt UA6, Ballochi G *et al* 1993 *Phys. Lett.* **317B** 243
Sozzi G *et al* 1993 *Phys. Lett.* **317B** 250
Bernasconi A *et al* 1988 *Phys. Lett.* **206B** 163
[13] Expt R108, Angelis A L S *et al* 1980 *Phys. Lett.* **94B** 106
[14] Expt R110, Angelis A L S *et al* 1989 *Nucl. Phys.* B **327** 541

Angelis A L S *et al* 1986 *Nucl. Phys.* B **263** 228
[15] Expt R806, Annassontzis E *et al* 1982 *Z. Phys.* C **13** 277
[16] Expt R806, Kourkoumelis C *et al* 1982 *Z. Phys.* C **16** 101
[17] Expt R807, Åkesson T *et al* 1985 *Phys. Lett.* **158B** 282
[18] Expt R807, Åkesson T *et al* 1990 *Sov. Jour. Nucl. Phys.* **51** 836
[19] Expt R807, Åkesson T *et al* 1986 *Z. Phys.* C **32** 491
[20] Expt UA2, Alitti J *et al* 1992 *Phys. Lett.* **288B** 386
Appel J *et al* 1986 *Phys. Lett.* **176B** 239 Alitti J *et al* 1991 *Phys. Lett.* **263B** 544
[21] Expt UA2, Ansari R *et al* 1988 *Z. Phys.* C **41** 395
[22] Expt UA1, Albajar C *et al* 1988 *Phys. Lett.* **209B** 385
[23] Expt CDF, Abe F *et al* 1994 *Phys. Rev. Lett.* **73** 2662
Abe F *et al* 1993 *Phys. Rev.* D **48** 2998
Abe F *et al* 1992 *Phys. Rev. Lett.* **68** 2734
[24] Expt CDF, Abe F *et al* 1993 *Phys. Rev. Lett.* **70** 2232
[25] Expt D0, Abachi S *et al* 1996 *Phys. Rev. Lett.* **77** 5011
[26] Aurenche P, Baier R, Douiri A, Fontannaz M and Schiff D 1984 *Phys. Lett.* **140B** 87
Aurenche P, Baier R, Fontannaz M and Schiff D 1988 *Nucl. Phys.* B **297** 661
[27] Baer H, Ohnemus J and Owens J F 1990 *Phys. Lett.* **234B** 127
Baer H, Ohnemus J and Owens J F 1990 *Phys. Rev.* D **42** 61
[28] Gordon L E and Vogelsang W 1993 *Phys. Rev.* D **48** 3136
[29] Gordon L E Argonne report ANL-HEP-PR-96-60
[30] Aversa F, Chiappetta P, Greco M and Guillet J P 1988 *Phys. Lett.* **210B** 225
Aversa F, Chiappetta P, Greco M and Guillet J P 1988 *Phys. Lett.* **211B** 465
Aversa F, Chiappetta P, Greco M and Guillet J P 1989 *Nucl. Phys.* B **327** 105
[31] Aurenche P, Chiappetta P, Fontannaz M, Guillet J P and Pilon E 1993 *Nucl. Phys.* B **399** 34
[32] Glück M, Reya E and Vogt A 1993 *Phys. Rev.* D **48** 116
[33] Berger E L and Qiu J 1990 *Phys. Lett.* **248B** 371
Berger E L and Qiu J 1991 *Phys. Rev.* D **44** 2002
[34] Gordon L E and Vogelsang W 1994 *Phys. Rev.* D **50** 1901
[35] Glück M, Gordon L E, Reya E and Vogelsang W 1994 *Phys. Rev. Lett.* **73** 388
[36] Vogelsang W and Vogt A 1995 *Nucl. Phys.* **453** 334
[37] Aurenche P, Baier R, Fontannaz M, Owens J F and Werlen M 1989 *Phys. Rev.* D **39** 3275
[38] Aurenche P, Baier R and Fontannaz M 1990 *Phys. Rev.* D **42** (1990) 1440
[39] Berger E L, Guo X and Qiu J 1996 *Phys. Rev. Lett.* **76** 2234
Berger E L, Guo X and Qiu J 1996 *Phys. Rev.* D **54** 5470
[40] Aurenche P, Fontannaz M, Guillet J P, Kotikov A and Pilon E 1997 *Phys. Rev.* D **55** 1124
[41] Glück M, Reya E and Vogt A 1995 *Z. Phys.* C **67** 433
[42] Glück M, Reya E and Vogt A 1992 *Z. Phys.* C **53** 127
[43] Stratmann M and Vogelsang W 1995 *Phys. Rev.* D **52** 1535
[44] Berger E L and Gordon L E 1996 *Phys. Rev.* D **54** 2279
Bailey B, Berger E L and Gordon L E 1996 *Phys. Rev.* D **54** 1896
[45] Martin A D, Roberts R G and Stirling W J 1995 *Phys. Lett.* **354B** 155
[46] Huston J *et al* 1995 *Phys. Rev.* D **51** 6139
[47] Baer H and Reno M H 1996 *Phys. Rev.* D **54** 2017
[48] Glück M, Reya E and Vogt A 1992 *Phys. Rev.* D **45** 3986
Glück M, Reya E and Vogt A 1993 *Phys. Rev.* D **46** 1973
[49] Glover E W N and Morgan A G 1994 *Z. Phys.* C **62** 311
Buskulic D *et al* (ALEPH Collaboration) 1996 *Z. Phys.* C **69** 365
[50] Lai H L *et al* (CTEQ Collaboration) 1995 *Phys. Rev.* D **51** 4763
[51] Glück M, Reya E and Vogt A 1992 *Z. Phys.* C **53** 651
[52] Martin A D, Roberts R G, Stirling W J and Sutton P J 1991 *Phys. Rev.* D **43** 3648
[53] Lafferty G D and Wyatt T R 1995 *Nucl. Instr. Meth.* A **355** 541
[54] Whalley M R 1995 HEPDATA: *World-Wide-Web User Guide* DPDG/95/01
[55] Whalley M R 1995 *A pocket guide to using the HEPDATA databases via TELNET* DPDG/95/01